Solvent dynamics in a glass-forming liquid from 300 K to 3 K

Lazonder, Kees; Pshenitchnikov, Maxim

Published in:
Chemical Physics

DOI:
10.1016/j.chemphys.2007.07.009

Publication date:
2007

Available online at www.sciencedirect.com
ScienceDirect
Chemical Physics 341 (2007) 123–142
Chemical Physics
www.elsevier.com/locate/chemphys

Solvent dynamics in a glass-forming liquid from 300 K to 3 K: What photon echoes can teach us

Kees Lazonder *, Maxim S. Pshenichnikov

Ultrafast Laser and Spectroscopy Laboratory, Zernike Institute for Advanced Materials, University of Groningen, Nijenborgh 4, 9747 AG Groningen, The Netherlands

Received 3 March 2007; accepted 6 July 2007
Available online 15 July 2007

Abstract

The temperature dependence of the optical non-linear response of dye molecules dissolved in a glass-forming liquid over a temperature range that includes the glass transition is investigated. Cooling down to temperatures below the glass transition dramatically slows the diffusive motion of the solvent molecules, while the bath retains its strong amorphous character. The results of ultrafast experiments such as echo-peak shift and heterodyne-detected echo are presented. The temperature dependence of the optical response is discussed within the context of the multimode Brownian oscillator model that is commonly used to describe dynamics in liquids. Freezing out a large part of the bath fluctuations allows for testing of the physical interpretation associated with this model. A temperature-dependent spectral density is proposed that can describe the results at all temperatures over the explored temperature range. The temperature dependence follows readily from the physical processes that are associated with the various parts of the density of states, with the exception of the fastest modes. The temperature dependence of these modes is inspected closely and the spectral shape is reinterpreted.

Keywords: Ultrafast; Photon echoes; Multimode Brownian oscillator; MBO; Liquid dynamics; Glass dynamics; Glass forming; Amorphous; Bath; Soft condensed matter; Spectral density; Temperature dependence; Glass transition; Underdamped; Overdamped; Non-condon effects

"*The echo of a distant time*"
Pink Floyd, *Echoes*

1. Introduction

Glasses are omnipresent in daily life. From high-tech computer memory elements, solar cells and optic fibers, to the low-tech application of many metal alloys, plastics and of course windowpanes, all these applications rely on glass-specific qualities [1,2]. For instance, the isotropic optical nature of a glass window pane is a direct result of the lack of translational long-range order, as are other macroscopic properties such as the low thermal conductivity. Even though glasses are utilized everywhere and anywhere in our daily lives, our understanding of these materials is quite limited. The principal question that remains is how the properties of a material, once the glass transition is passed, can suddenly change so drastically without a major structural rearrangement on a molecular level.

If the cooling rate is high enough, a liquid can be cooled to a super-cooled state where the properties of the substance are still those of a liquid, although the temperature is lower than the freezing point [3]. When the temperature is lowered further, its volume keeps decreasing continuously. At some point, the cooling results in a drastic increase in the viscosity of the super-cooled liquid. This is where the glass transition temperature T_g is reached. Below this temperature the substance is in the glass state and the thermal expansion rate is smaller than that of the liquid. The liquid-to-glass transition is an example of a higher-order phase transition since derivative functions of the chemical potential, such as volume, entropy, enthalpy

* Corresponding author.
E-mail addresses: lazonder@gmail.com (K. Lazonder), M.S.Pshenitchnikov@RuG.nl (M.S. Pshenichnikov).

0301-0104/$ - see front matter © 2007 Elsevier B.V. All rights reserved.
doi:10.1016/j.chemphys.2007.07.009

and heat capacity change, continuously at a narrow temperature interval as they do not in a first-order phase transition [4].

The precise temperature at which the liquid-to-glass transition occurs depends on the cooling rate. At some point molecular motions become so slow that a time-independent equilibrium state can no longer be maintained. In other words, the system reaches a non-ergodic state, since the precise condition is dependent on the thermal history of the sample. For different cooling rates this occurs at different temperatures, hereby causing the small variation in glass transition temperatures. Typically, variation of the cooling rate by an order of magnitude changes the glass temperature by a few Kelvin. This hampers a consistent definition of the glass transition temperature [5–7].

Most of the current theories on glass formation concentrate on the ergodicity-breaking aspect of the glass transition; the focus is on the kinetic events that lead to the thermodynamic change of state. The thermodynamic aspects of the transition can be illustrated by observing the change in entropy of a super-cooled liquid, cooled down from the freezing point to the glass temperature, in comparison with that of the corresponding crystal at the same temperature. The entropy of the super-cooled liquid, although much higher at first, decreases more rapidly and approaches the entropy of the crystal because the specific heat of the liquid is larger than that of the crystal. The temperature at which the entropies of both phases would be equal is called the Kauzmann temperature T_K. The entropy of the super-cooled liquid would even reach a negative value at a finite temperature if the temperature was lowered below this point (the so-called Kauzmann paradox [8]). Since the existence of an amorphous phase with lower entropy than the well-ordered crystalline phase is unphysical, a pronounced change in the specific heat has to occur before this temperature is reached, i.e. the glass transition. This fact sets up a lower limit on the glass temperature, independent of the cooling rate, and highlights the underlying thermodynamic basis of the transition [9,10].

Although the nature of the glass transition is still not completely understood, significant advances have been made in this field in recent times [5]. In the high-temperature regime well above the glass temperature, upon cooling, the liquid becomes viscous but is always ergodic; its properties have no history dependence. The dynamics of the system in this region are described by means of a model based on molecular collisions. At the highest temperatures the system is expected to respond on perturbations with relaxation times that depend exponentially on temperature, i.e. with a normal Arrhenius-type dependence.

This changes however, when the temperature is lowered further. Dielectric relaxation, viscosity, diffusion and other parameters connected to molecular mobility need to be described within another framework in this region, since the observables show deviations from an Arrhenius-type temperature dependence. In absence of a complete description of glass formation a plethora of equations is used to fit experimental temperature dependence of relaxation rates. From these the Vogel–Fulcher (VF) equation is the most famous [11,12]. It models non-Arrhenius behavior by assuming a divergence temperature at which all relaxation comes to a halt. This divergence temperature, however, usually deviates substantially from the glass temperature [13–17]. Furthermore, besides the temperature dependence of the relaxation rates, the relaxation functions themselves become non-exponential with time in this regime, which is an indication of the existence of distributions of relaxation regimes in the liquid [18].

At the temperature of the actual transition not only does the history of the studied material influence the observables of interest, but also the timescale of the perturbation and the measurement itself influence these observables. The common methods for describing relaxation dynamics are no longer practical since they can only be effectively applied over limited temperature intervals and timescales. The widespread assumption [19–24] is that the non-exponential relaxation processes with respect to temperature and time are strongly influenced by the underlying potential energy landscape spanned by all the degrees of freedom it has. Landscape paradigms are commonly used to describe the qualitative behavior of complex systems [25]. In the case of amorphous materials, the shape of the landscape in the vicinity of its configurational state and particularly the height of surrounding barriers and ridges determine the amount of configurational space the system can explore. Evidence is mounting [26,27] that the onset of non-exponential relaxation corresponds to a well-defined cross-over temperature (well above the glass temperature) below which the system can no longer freely explore all configurational space but instead is confined to deep basins in the landscape. At lower temperatures the system is trapped in the lowest accessible part of such a basin.

The chemical reactivity of some reactant dissolved in a liquid or a glass as well as the spectroscopic characteristics of a dye molecule in solution are strongly affected by the interactions between solute and solvent. The dynamics of these interactions lead to fluctuations of the energy levels of the relevant electronic states of the solute. The optical dynamics are therefore key to understanding the solute's reactivity in the condensed phase. The fluctuations of the energy levels can make reacting systems cross potential energy barriers and subsequently dissipate excess energy. Furthermore, the solvent–solute interactions can allow for coupling of states, and thus create reaction pathways, that would otherwise not occur. In spectroscopy, these fluctuations create variations in the size of the energy gap associated with the optical transitions. In steady-state optical experiments this usually yields broad featureless spectra that mask the underlying dynamics with very little difference between the optical properties of a chromophore dissolved in a glass or in a liquid [28,29]. The broad spectra are a measure of the amplitude of the frequency fluctuations of the optical transition, which depends on the variations in direct surroundings of the individual

chromophores. Since the amorphous character in both phases of a certain solvent is similar, so are the linear spectra. However, the dynamics that are hidden beneath the linear spectra differ fundamentally, and various models exist that describe the temporal changes of the involved transition frequencies.

The energy gap dynamics can be probed by the non-linear optical techniques such as three-pulse echoes (3PE), three-pulse echo-peak shift experiments (3PEPS) and heterodyne-detected photon echoes (HDPE) [30,31]. The above mentioned non-linear spectroscopic techniques essentially measure the decay of quantum mechanical coherences due to solute–solvent interactions. Since it is not practical to treat all of the solvent degrees of freedom explicitly, a density matrix approach is generally used to average over the less important bath degrees of freedom, while treating the solute and the most relevant modes of the solvent in a more detailed fashion. The multimode Brownian oscillator (MBO) model for example allows for a simple interpretation of system-bath dynamics in terms of overdamped and underdamped harmonic oscillators [30,32]. The oscillators can be viewed as solvent (or solute) degrees of freedom that are strongly coupled to the electronic states of interest. The optical coherence decays on a number time scales varying from tens of femtoseconds to milliseconds. The set of oscillators needed to adequately describe this coherence loss can be expressed as a spectral density (SD) of states, and the various features in this distribution can be assigned to specific aspects of system-bath dynamics. The MBO model has also been tested at lower temperatures [30,32–35].

On the experimental side, as the fastest dynamics in liquids or glasses at room temperatures occur at a 10's of fs timescale, one needs an adequate femtosecond time resolution to follow the dynamics in real time. Weiner et al. were the first to study the temperature dependence of the 3PEPS in a glass host [36,37]. In the 3PEPS experiment, the maximum of the time-integrated echo signal from zero delay is measured at a certain waiting time as a function of the temperature. A linear increase of ~30 fs of the echo-peak shift was found when cooling a polymethyl methacrylate (PMMA) sample doped with cresyl violet from 290 K to 15 K. This was explained as a transition from homogeneous (i.e., fast environmental fluctuations at any relevant experimental timescale) to inhomogeneous (i.e., a static distribution of transition frequencies) broadening due to smearing of the vibrational structure of individual dye molecules. Despite the clearly resolved echo-peak shift in the low temperature scattering data, a pronounced echo tail, indicative of a long dephasing time T_2, was not observed. The waiting time measurements at a fixed temperature did not show any appreciable changes in the echo-peak position which was interpreted as indication that spectral diffusion does not play a major role in the polymer matrix.

In a later study by Bardeen et al. [38,39] the two-pulse echo (2PE) and the 3PE response of two other dyes, Oxazine 4 and Styryl 7, dissolved in both PMMA and polyvinyl alcohol were measured for temperatures from 30 K to 300 K. The echo decays in the case of the Styryl dye were too fast to be discussed in a meaningful way at any temperature. In the case of the Oxazine dye, the signal was interpreted as a combination of one dominant vibrational mode and a single exponential decay of the polarization. A linear dependence of the dephasing rate associated with this exponential decay with temperature was found. The authors remarked that this is consistent with linear coupling of the transition to the phonon bath when the so-called high-temperature limit (i.e. $kT \gg \hbar\omega$) is valid for all phonons at all temperatures. This implies that the dephasing is caused by low-frequency modes, that is, by those modes whose frequencies lie well below 20 cm^{-1}. However, the dephasing time caused by these modes in the echo decays was measured as ~50 fs, which corresponds to phonon frequencies in the range of 1000 cm^{-1}. Therefore, the system's frequency fluctuations appear to be Markovian when the correlation time is considered, and should thus be described using high frequency modes. Hence, there exists an apparent incongruity between the linear temperature dependence of the dephasing rates and the Markovian character of the echo decays. The authors suggested that the linear coupling representation as implied by the MBO model is inadequate, and that quadratic or higher coupling terms need to be considered.

On the other hand, Nagasawa et al. [40–42] concluded that the MBO model should still be readily applicable to describe the optical dephasing of the infrared dyes IR144 and DTTCI dissolved in polyvinylformal and PMMA down to temperatures of 30 K. Besides considering the 3PE signal and the absorption spectrum, they also studied the 3PEPS and transient grating scattering, which afforded a more detailed analysis of the temperature dependence of the modes involved in the optical dephasing process. The experiments revealed an initial decay of the echo-peak shift that could be modeled by assuming fast dephasing of intramolecular vibrational wave packets and an inertial solvent response, followed by quantum beats originating from the prominent intramolecular modes of the dye. Nagasawa et al. found that in these glasses the inertial response was best modeled using a severely damped oscillator to allow for some undershoot in the echo-peak shift data. At the same time they indicated that the precise characterization of this mode is limited by the resolution obtained in the analysis of the experimental data. Contrary to the experiments by Bardeen et al., the detailed computer simulations showed that the echo-peak shift signal, the absorption and Raman spectra could be self-consistently reproduced at all temperatures, by assuming a fixed spectral density in terms of the MBO model. Furthermore, according to the experiments by Nagasawa et al. the relatively weak coupling of DTTCI to its vibrational and bath modes results in a more prominent temperature dependence of the echo-peak shift when compared with other dyes like IR 144.

Optical dephasing of zinc–octaethylporphine in several glass-forming liquids at temperature from 0.35 K to a maximum of 100 K was investigated by Vainer and Gruzdev

[43–48] using narrowband two-pulse and incoherent photon echoes. They were able to distinguish between a low temperature range, where dephasing mechanisms related to tunneling of the system to nearby almost degenerate minima in the energy landscape were dominant, and a higher temperature range where the dephasing was best described by the coupling of the chromophore to one or two low-frequency vibrational bath modes.

Summarizing the literature review, almost all previously reported studies concentrated on polymer solvents that show no phase transition in the temperature range under consideration. With respect to the bath dynamics, the polymer host can be considered similar to a glass. Only the above mentioned narrowband studies by Vainer and Gruzdev et al. used a simple glass-forming liquid and a wide temperature range, but these studies were also conducted at temperatures that were below the glass transition at all instances. No glass transition occurred in the temperature ranges that have been studied, and experimentally, no major deviations from theoretical predictions for the line broadening have been reported.

In this paper the temperature dependence of solvent dynamics in a glass-forming host is studied using a number of steady-state and ultrafast four-wave mixing spectroscopic techniques from room temperature down to the cryogenic regime. The applied temperature range includes a phase transition of the solvent at 150 K where all diffusive solvent motion slows down to a completely static state of affairs. The results of temperature-dependent echo-peak shift and heterodyne-detected photon echo experiments in glass-forming liquids are reported. The limits wherein the ability of the MBO model to accommodate temperature changes with a temperature-independent spectral density are discussed. It is found that the temperature dependence of the MBO parameters matches largely the expected temperature dependence of the microscopical physical processes that underlie the modes in question. However, the fastest mode that is frequently associated with dephasing of the vibronic manifolds does not depend on temperature in a way that is characteristic for an MBO mode. Therefore, this mode is attributed to anharmonic coupling of pseudo-local phonon modes to the electronic transition, since its temperature dependence ties in with such or a similar mechanism much better.

2. Theory

Even without choosing a particular model for the solute–solvent interactions the optical response in a time-resolved optical experiment can be defined in terms of a normalized autocorrelation function of the energy gap using very general arguments. The echo experiments in this paper are also described in terms of the same two-time correlation functions of the energy gap:

$$M(t_1,t_2)=\frac{\langle \delta\omega(t_2)\delta\omega(t_1)\rangle}{\langle \delta\omega(t_1)^2\rangle}, \tag{1}$$

where $\delta\omega(t)$ is the time-dependent optical transition frequency of the solvated molecule and the brackets indicate a statistical average over the ensemble. Various models can be applied for relating the correlation function to the physical processes of bath dynamics. The phonon-based harmonic mode models are well-established descriptions for solvation dynamics in the high-temperature high-fluidity regime. It makes sense to only consider a few relevant solvent modes explicitly in the Hamiltonian instead of all possible bath modes. In the MBO model this is done by coupling the adiabatic eigenstates of the optical system linearly to a limited number of nuclear harmonic oscillator modes. These modes can then either depend on the nuclear state of the system or also couple to the system in precise the same way as a Gauss–Markov heat bath would [30,34]. Here we present a brief overview of the MBO model; for more details the reader is redirected to the book by Mukamel [30].

In the MBO model the system is described as a two level Hamiltonian, but now coupled to a number of harmonic oscillators that describe the nuclear coordinates $\mathbf{Q}_B$ of the bath:

$$\begin{aligned}\widehat{\mathbf{H}}_{\mathrm{tot}} &= |g\rangle[\widehat{\mathbf{H}}_g(\mathbf{Q}_S)+\hat{\mathbf{h}}_g(\mathbf{Q}_S,\mathbf{Q}_B)]\langle g| + |e\rangle[\widehat{\mathbf{H}}_e(\mathbf{Q}_S)\\ &\quad +\hat{\mathbf{h}}_e(\mathbf{Q}_S,\mathbf{Q}_B)]\langle e|.\end{aligned} \tag{2}$$

For convenience the system modes are described as two linearly displaced harmonic potentials:

$$\widehat{\mathbf{H}}_{e,g}=\frac{P^2}{2m}+\frac{m\omega_0^2}{2}(Q+D_{g,e})^2. \tag{3}$$

The system with momentum P, coordinate Q, mass m, frequency ω_0 and displacement D ($D_g\equiv 0$) couples to a number of N harmonic modes

$$\widehat{\mathbf{h}}(\mathbf{Q}_S,\mathbf{Q}_B)=\sum_{i=1}^{N}\frac{p_i}{2m_i}+\frac{m_i\omega_i^2}{2}\left(q_i+\frac{c_iQ}{m_i\omega_i}\right)^2, \tag{4}$$

that in turn have momentum, coordinate, mass, frequency and also a coupling constant c_i. These modes result in a damping of the harmonic oscillator that is usually taken to be independent of its frequency

$$\gamma_i(\omega)=\frac{c_i^2}{2m_i\omega_i^2}\delta(\omega-\omega_i)\approx\gamma_i. \tag{5}$$

Moreover, since the two potentials of the harmonic chromophore are linearly displaced, any change in its coordinates will result in an energy fluctuation that depends on the displacement. In this idealized case, all the solvent dynamics are related to a correlation function of the energy gap through the spectral density of states. In the MBO model it is simply supposed to consist of a number of harmonic modes:

$$C(\omega)=\sum_i^N C_i(\omega)=\frac{2}{\pi}\sum_i^N\frac{\lambda_i\omega_i^2\gamma_i\omega}{(\omega_i^2-\omega^2)+\omega^2\gamma_i^2}. \tag{6}$$

A defining point of the MBO model is that it treats the system as two identical harmonic potentials that couple linearly to the harmonic bath modes. The coupling term $\hat{\mathbf{h}}(\mathbf{Q}_S, \mathbf{Q}_B)$ in the Hamiltonian of Eq. (2) is expressed using a cumulant expansion that is cut off after the linear term. At room temperature when the bath fluctuates fast and with nearly identical potential energy surfaces of the system's ground and excited state, this is a reasonable approximation. In the case that the ground and excited-state propagate differently in time or when the fluctuations are slower, so that the fluctuation dissipation theorem does not hold, however, higher-order coupling terms might need to be considered.

The key experimental observable in this paper is the photon echo signal. It is proportional to the third-order optical polarization that can be expressed as a convolution of the three incident fields and the non-linear system response function $R^{(3)}$ [30]:

$$P^{(3)}(\mathbf{r},t) = \int_0^\infty \mathrm{d}t_3 \int_0^\infty \mathrm{d}t_2 \int_0^\infty \mathrm{d}t_1 R^{(3)}(t_3,t_2,t_1) E_1(\mathbf{r}, t-t_3) \times E_2(\mathbf{r}, t-t_3-t_2) E_3(\mathbf{r}, t-t_3-t_2-t_1). \quad (7)$$

The third-order response function $R^{(3)}$ is determined by the dependence of the nonlinear susceptibility on the material parameters as the transition dipole moments and electronic energy levels of the chromophores, and is therefore influenced by all nuclear and electronic motions and relaxation processes of the system.

The stochastic averaging over all possible frequency fluctuations $\delta\omega$ indicated by the brackets in Eq. (1), can be performed in various ways. The method of choice depends on the knowledge of the physics of the fluctuations. When the fluctuations are random, with frequency offsets probabilities that can be described by a time-independent normal distribution, the exponential terms that make up the above system response can be expanded into a Taylor series. The terms of the expansions are subsequently rearranged as a sum of two-time correlation functions. In the MBO model the averaging and integration can be performed and the results is expressed as a line broadening function $g(t)$:

$$\left\langle \exp\left[-\mathrm{i}\int_0^\tau \mathrm{d}t \delta\omega(t)\right]\right\rangle = \exp[-g(t)]. \quad (8)$$

Since the evolution of the bath states in this model also depends on the system evolution, line broadening function is, in general, a complex quantity:

$$g(t) = \Delta^2 \int_0^t \mathrm{d}\tau_1 \int_0^{\tau_1} \mathrm{d}\tau_2 M'(\tau_2) - \mathrm{i}\lambda \int_0^t \mathrm{d}\tau [1 - M''(\tau)]. \quad (9)$$

Two static parameters, λ and Δ are the reorganization energy due to the relaxation of the bath upon a change of state of the system, and the root mean square of amplitude of the frequency fluctuations, respectively. The correlation functions $M'(t)$ and $M''(t)$ are connected to the SD as follows:

$$M'(t) = \frac{1}{\Delta^2}\int_0^\infty \mathrm{d}\omega \frac{C(\omega)}{\omega} \coth\left[\frac{\hbar\omega}{2k_\mathrm{B}T}\right]\cos[\omega t], \quad (10)$$

$$M''(t) = \frac{1}{\lambda}\int_0^\infty \mathrm{d}\omega \frac{C(\omega)}{\omega}\cos[\omega t]. \quad (11)$$

The parameters Δ and λ can be calculated from Eqs. (10) and (11), respectively, by recalling that both correlation functions are normalized to unity at zero time.

Since the SD $C(\omega)$ is assumed to be temperature independent when dealing with harmonic potentials, population changes among the states, represented through the hyperbolic cotangent term, introduce the temperature dependence expected in the MBO model. From a practical point of view, the temperature independence of the spectral density makes it more convenient observable than the correlation function.

When calculating the third-order optical response function, a combination of Brownian oscillators (BO's) can be used to make up the spectral density. These modes can have different characteristics depending on their damping factors, amplitudes, etc. The resulting spectral density is simply the sum of the various modes as in Eq. (6). It has been shown that there are three main types of oscillators that are needed to accurately describe the signal in the experiments with femtosecond pulses. First of all, prominent quantum beats in the echo signals are indicative of intramolecular vibrational dynamics that are described by underdamped Brownian oscillator (UBO) modes ($\gamma_i \ll \omega_i$):

$$C(\omega) = \frac{\lambda_i}{2\pi}\frac{\omega_i\gamma_i}{(\omega_i-\omega)^2 + (\gamma_i/2)^2}. \quad (12)$$

The associated coupling strength parameters are interrelated through:

$$\Delta_i^2 = \int_0^\infty C(\omega)\coth\left[\frac{\hbar\omega}{2k_\mathrm{B}T}\right] = \lambda_i\omega_j\coth\left[\frac{\hbar\omega_j}{2k_\mathrm{B}T}\right]. \quad (13)$$

These modes are dependent on the type of chromophores used and nearly independent of the type of solvent, and therefore their intramolecular character is broadly acknowledged.

Secondly, the correlation function typically decays on a number of times scales, varying from 100's fs to over 100's ps depending on the solvent. These modes are generally associated with diffusion like solvent motion and are expressed as several strongly overdamped ($\gamma_i \gg \omega_i$) oscillators:

$$C_i(\omega) = \frac{2\lambda_i\Lambda_i\omega}{\pi\left(\Lambda_i^2+\omega^2\right)}, \quad (14)$$

where $\Lambda_i = \omega_i^2/\gamma_i$. The strongly overdamped Brownian oscillator (SOBO) is very useful for understanding solvent dynamics because when the high-temperature limit (HTL) applies, i.e. $\hbar\Lambda_i/k_\mathrm{B}T \ll 1$, it yields a simple inverse correlation time of the system-bath fluctuations. In the HTL, the relation between the two normalization constants becomes

$$\Delta_i^2 = \frac{2k_B T\lambda_i}{\hbar}. \tag{15}$$

This type of oscillator is used to describe the effects of spectral diffusion. Two or three of such SOBO oscillators are often needed to adequately model the correlation function in echo experiments. The correlation times of these modes are strongly solvent dependent. It is important to realize that for low temperatures the validity of the high-temperature limit has to be verified. Static inhomogeneity is also modeled with a SOBO oscillator with a correlation time that is much longer than the longest experimental timescale.

Thirdly and finally, an ultrafast decay is found for all solutes in all solvents on the time scale of tens of femtoseconds. The fastest part of this decay is usually attributed (at least, in part) to a free-induction type decay due to impulsive excitation of the vibronic manifold, as known from the theory of radiationless processes [49]. Since this decay occurs almost on the same timescale as the resolution of the femtosecond experiments, it is often not included in MBO analysis. This is because at the shortest timescales, the analysis of correlation function through echo signals is complicated.

Besides this intramolecular decay, the fastest of the solvent modes decays on a typical timescale of about 100 fs. Therefore, this remaining part of the ultrafast decay is often linked to inertial solvent motions that happen when the first shell of solvent molecules reacts to the change in the electronic state of the chromophores. Both these fast decays can be modeled using a Gaussian spectral distribution (GSD) of undamped ($\gamma_i = 0$) oscillators:

$$C(\omega) = \frac{2\lambda_i\omega}{\sqrt{2\pi}\omega_0}\exp\left[-\frac{\omega^2}{2\omega_0^2}\right]. \tag{16}$$

This contribution to the spectral density is often used to relate the ultrafast decay to the solvation frequency (ω_0) that is found in molecular dynamics simulations of solvent dynamics [50–54]. In several studies, it was noted that the time scale of the inertial solvent response is similar for different solvents and that the precise spectral shape of the contribution is not vital when describing the data [41,55,56]. For instance, in polymers a decay on a similar timescale is often described using a single strongly damped oscillator.

Concluding this section, we note that the part of the spectral density that is covered by the group of SOBO's and one of the fast GSD modes is considered to describe pure solvent dynamics. The similarities of this part of the spectral density with the pure solvent spectral densities probed by Raman experiments and especially optical Kerr effect (OKE) experiments are striking, although there is no proven theoretical correspondence between the echo and the neat solvent experiments [40,57–62]. Due to the abstract nature of this type of model for solvent dynamics, one learns little about the precise origins of this part of the correlation function, although the evidence seems to suggest collision induced phase relaxation. Therefore, temperature-dependent measurements should be instructive in further identifying the underlying processes.

3. Experimental

The laser used in the femtosecond experiments was a cavity-dumped Ti:sapphire oscillator pumped by a Spectra Physics Millennia Nd:YVO_4 laser [63,64]. The acousto-optical Bragg cell was operated in a double-pass geometry with its folding mirrors in a confocal position and driven by a 5 W electronic driver (CAMAC systems). Dumping efficiencies up to 80% with contrast ratios with preceding and succeeding pulses to over 10^3 were achieved. The laser typically generated 40 nJ, 14 fs pulses at a 10 kHz repetition rate.

The pulses produced by the cavity-dumped laser were pre-compressed by double-passing the laser output through two fused-silica prisms to attain the shortest pulses in the sample. Four pulses were used in the heterodyned femtosecond echo experiments, three excitation pulses and a local oscillator pulse (Fig. 1). The pulses were timed using 0.1 μm precision delay stages (Newport) and subsequently focused in the sample with 125 mm focal length singlet lenses. One of the pulse trains was modulated by a mechanical chopper.

The sample was mounted in an Oxford Instruments Variox helium cryostat. The temperature in the cryostat could be varied to any temperature from 300 K to 1.7 K using either liquid nitrogen or liquid helium as a cooling agent. The temperature could be stabilized using an active temperature controller (Oxford Instruments) with a 0.1 K precision. The total amount of dispersive material in the optical path of all beams before the cryostat was carefully equalized using compensating plates. Cross-correlations of all possible combinations of pulses were measured inside the cryostat either by mounting a two-photon photodiode on the sample rod [65], or by using a 100 μm KDP crystal with subsequent detection of the second harmonic. These measurements indicated that high-order contributions to the dispersion by the cryostat windows did lead to slight (~15–20%) broadening of the excitation pulses at the place of the sample position.

The echo signals were detected by photodiodes and processed through two lock-in amplifiers. Stray light was

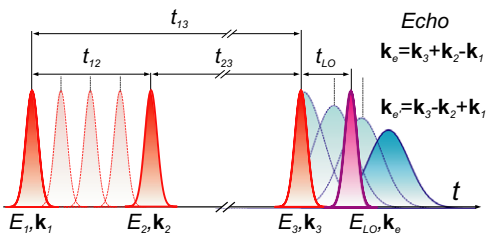

Fig. 1. The pulse sequence as used in the experiments. The two echo signals in conjugated directions $\mathbf{k}_e = \mathbf{k}_3 + \mathbf{k}_2 - \mathbf{k}_1$ and $\mathbf{k}_{e'} = \mathbf{k}_3 - \mathbf{k}_2 + \mathbf{k}_1$ were detected simultaneously.

blocked using a mask and detecting at a 2 m distance via pick-up mirrors and occasionally via a spatial filter. Data collection and the control of the delay stages was computer controlled. All experiments could be run in a completely automated manner without intervention of the experimentalist.

Solutions of 3,3′-diethylthiatricarbocyanine iodide (DTTCI, Lambda Physik) in a 1:1 volume mixture of ethanol and 1,2-propanediol with an optical density of ~0.15 at the absorption maximum at 77 K were used as sample material. The dye was chosen for its spectrum that matches the excitation spectrum, solubility, photo-stability and for the experience that had already been gathered using this dye in room-temperature photon echo experiments [63,67,68]. The solvent was chosen for the optical quality of the glasses it forms. The sample was mounted in a 1 mm quartz cuvette. After cooling down, the sample was left to settle for at least an hour. Note that with the development of cooling techniques with rates well over 10^6 K s^{-1} [70], it is now generally believed that all condensates can be prepared as a glass [6,7]. Therefore, formally speaking, the term "a glass-forming liquid" is somewhat misleading since glasses can be produced from all liquids. Nonetheless, the term will be used here to identify those liquids that form glasses already at relatively low cooling rates, about 10^{-5}–10^{-1} K s^{-1} [71]. This is particularly true for liquids that have a value of the ratio of boiling to freezing temperatures that is larger than 2.0 such as the ethanol/propanediol mixture used in the present experiments [72].

To make sure no sample heating effects occur, the excitation pulse intensity never exceeded 1 nJ, and usually were ~500 pJ at the sample. Also, the repetition rate was kept at 10 kHz. At these pulse energies an estimate suggests that transient temperature effects play no role in our experiments [73,74]. Notwithstanding the low pulse energies, at temperatures below 80 K and right above the glass temperature (at 150 K, see below), where the heat capacity of the sample was small, some bleaching occurred over the time scale of several scans ($\frac{1}{2}$ hour). To counteract this, the sample was moved within the cryostat to refresh the sample in the focal volume.

The following two main scenarios were utilized experimentally. First, time-integrated echo signals with the local oscillator blocked were measured in the phase-matched directions (Fig. 1) by square-law detectors:

$$S_{\text{homodyne}}(t_{12}, t_{13/23}) \propto \int \left|P^{(3)}(t; t_{12}, t_{13/23})\right|^2 \mathrm{d}t. \tag{17}$$

Typical traces, collected in such an experiment when the time between the first two pulses t_{12} (the coherence time) was scanned, are depicted in Fig. 2a. Specifically, the two traces represent the scan with the timing t_{13} between the first and the third pulse fixed and the scan with the timing t_{23} (the waiting time) between the second and third pulse fixed. This yields an echo signal respectively in the $\mathbf{k}_{e'}$ and the $\mathbf{k}_e$ direction (Fig. 1). If similar scans are repeated at different waiting times t_{13} and the echo maximum in the t_{12}-direction is plotted as a function of the time t_{13}, we arrive at the echo-peak shift experiment. To establish the position of the echo maximum, the traces are usually fitted with a Gaussian profile. To allow for asymmetric profiles at short waiting times, the traces were subsequently fitted with a third-order polynomial around the first guess of the maximum to pinpoint the maximum more precisely. The echo-peak shift is half of the distance between the maxima of the two traces and was plotted against the waiting time.

Another arrangement of this same scenario is realized when the time t_{12} is set at a certain value while the delay t_{13} is scanned. This records the so-called longitudinal echo scan. A particular case of such strategy is well-known transient grating experiment ($t_{12} = 0$).

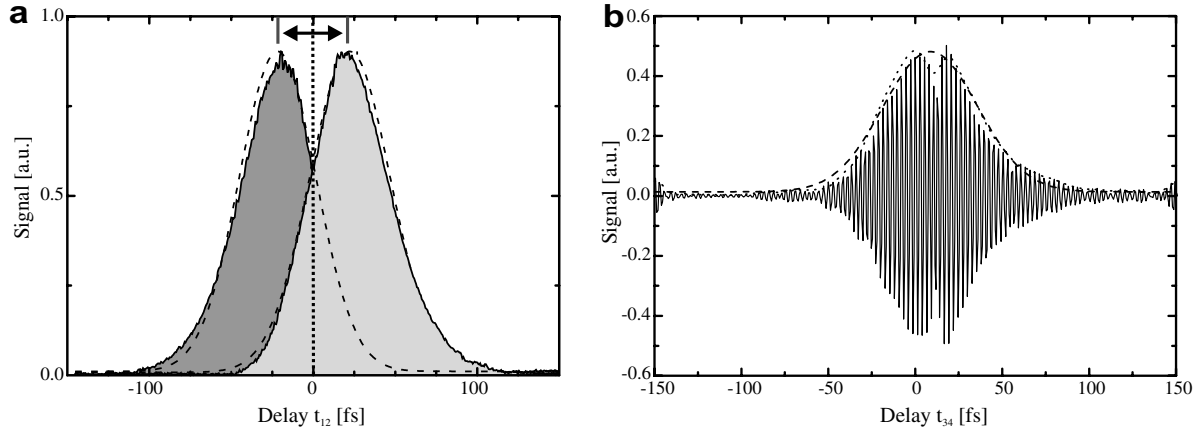

Fig. 2. (a) Typical echo-peak shift traces. The light grey trace is an echo signal as a function of the coherence time t_{12} with the time t_{13} between pulse 1 and 3 fixed, detected in the $\mathbf{k}_e$ direction. The dark grey trace is an echo signal with the time between pulse 2 and 3 fixed, detected in the $\mathbf{k}_{e'}$ direction. The dashed curves are Gaussian fits. The arrow indicates approximately two times the echo-peak shift. (b) Typical heterodyned echo signal. The delay of the local oscillator t_{34} is scanned and the other pulse timings are: $t_{12} = 10$ fs, $t_{13} = 210$ fs. The dotted curve represents the Fourier filtered signal (i.e., the signal envelop) while the dashed curve is the Gaussian fit. The sample temperature is 300 K.

The second experimental scenario implies that one of the echo signals is mixed with a fourth pulse, the so-called local oscillator. The detected signal becomes proportional to the product of the emitted echo field and the local oscillator field:

$$S_{\text{heterodyne}}(t_{12}, t_{23/13}, t_{34}) \propto \int_0^\infty \mathrm{Re}[P^{(3)}(t; t_{12/13}, t_{23}) \times E^*_{\text{LO}}(t - t_{34})]\,\mathrm{d}t. \quad (18)$$

Since $|E_{\text{LO}}| \gg |P^{(3)}|$, this greatly enhances the signal and facilitates detection even in situations when a lot of stray light is present. Due to the fact that fluctuations of the local oscillator are directly detected, best results are obtained with weak local oscillator pulses, typically attenuated by 3–4 decimal orders of magnitude compare to the excitation pulses. Most importantly, the local oscillator allows detection of the temporal profile and phase of the echo signal that contain essential information about the system dynamics. Although the temporal phase is not used in this study, the echo profile will be shown to be indispensable in revealing the glass transition.

A typical heterodyned echo trace is shown in Fig. 2b. In such an experiment, the time delays t_{12} and t_{23} were set at desirable values, and the time t_{34} is scanned. To extract the actual echo profile, the pump–probe background contribution was subtracted by fitting the data with a slowly varying polynomial and subsequent removal of this baseline. The carrier frequency component was eliminated from the signal using a digital Fourier filter. The resulting profile was fitted with a Gaussian in order to obtain the position of the maximum of the profile, its width, and height.

The conventional requirement to setups for heterodyne detection is interferometric stability during experiments. However, the procedure of the signal processing used here, implies that the setup maintains such stability only within a single t_{34} scan (about a minute). This allowed us omitting any experimentally complex active interferometric stabilization of the setup [67].

4. Results

In this section we discuss the results obtained from a variety of spectroscopic techniques on a DTTCI chromophore incorporated into the liquid/glass matrix. After a brief overview of the main experiments performed, we first focus our attention on the adequate description of the room-temperature data. With these in hand, the MBO analysis will be extended onto the lower temperatures by introducing temperature variance of the MBO modes.

4.1. Overview of the experiments

An overview of the main experiments that are considered when obtaining the SD is displayed in Fig. 3. These plots are meant to give a concise outline of the effects of temperature on the outcome of the various spectroscopic experiments.

The absorption spectrum of DTTCI in EtOH/PD in Fig. 3a shows narrowing of the bands with decreasing temperature. Where at 300 K the full width at half maximum (FWHM) of the spectrum is approximately 450 cm^{-1}, at 100 K this is reduced to $\cong$330 cm^{-1} and at 3 K it is only $\cong$260 cm^{-1}. The spectrum also exhibits a small red-shift of $\cong$65 cm^{-1} at the lower temperatures.

Typical time-integrated three-pulse echo traces at various temperatures are shown in Fig. 3b. The increasing inhomogeneous character of the solvation dynamics with decreasing temperature is obvious from the echo signals; they become wider, more asymmetric, and they peak at a later time. Whereas at 300 K the echo is approximately 40 fs wide, at 3 K this has become $\cong$80 fs at FWHM. The echo maximum shifts from nearly 9 fs at room temperature to over 22 fs at 3 K. Although the echo stretches to longer times at lower temperatures, the nanosecond decays observed in the experiments with picosecond pulses are not present here [28,74].

The echo-peak shift measurements as a function of the waiting time t_{13} reflect the above temperature dependence as illustrated by Fig. 3c. As the temperature drops, the dynamics become visibly slower, and correspondingly the echo-peak shift increases. The signal decays fast at short times which at first glance seems to be temperature independent. A region that is characterized by several recurrences of the echo-peak shift follows this decay. These quantum beats, which are caused by the intramolecular vibrational motions of the chromophores [31,55,56,66–69], do not change their frequency substantially at lower temperature but seem to increase in amplitude while the damping of the vibrations seems to slow down. The long tail of the echo-peak shift signal is an indication of the coupling of the chromophore to diffusional modes of the solvent. This part of the echo-peak shift function shows the increased static portion of the correlation function with decreasing temperature by becoming nearly constant. This decrease of the slope at times longer than 2 ps clearly indicates that the modes related to diffusional solvent motion are frozen out.

The effects of temperature on the vibrational dynamics can be readily observed in the 3PEPS traces in Fig. 3c as the quantum beats become more prominent at lower temperatures although little seems to change as soon as the glass temperature is passed ($T_g = 150$ K). This lack of change below T_g is the first signature of the glass transition that is apparent from superficial inspection of the experimental data (*vide infra*). Fitting the traces with exponentially damped cosine functions yields the relative amplitudes, frequencies and decays of the three main vibrational modes: 0.9, 150 cm^{-1}, 150 fs; 0.03, 380 cm^{-1}, 500 fs; and 0.07, 485 cm^{-1}, 700 fs, respectively. These values corroborate well with the previously published data [31,67,68,75], and will be rectified later while applying the full-scale modeling. As has been suggested earlier, the waiting time of 210 fs offers an outstanding opportunity to suppress the intramolecular vibrational contribution onto the experimental observables. First, at this time the most

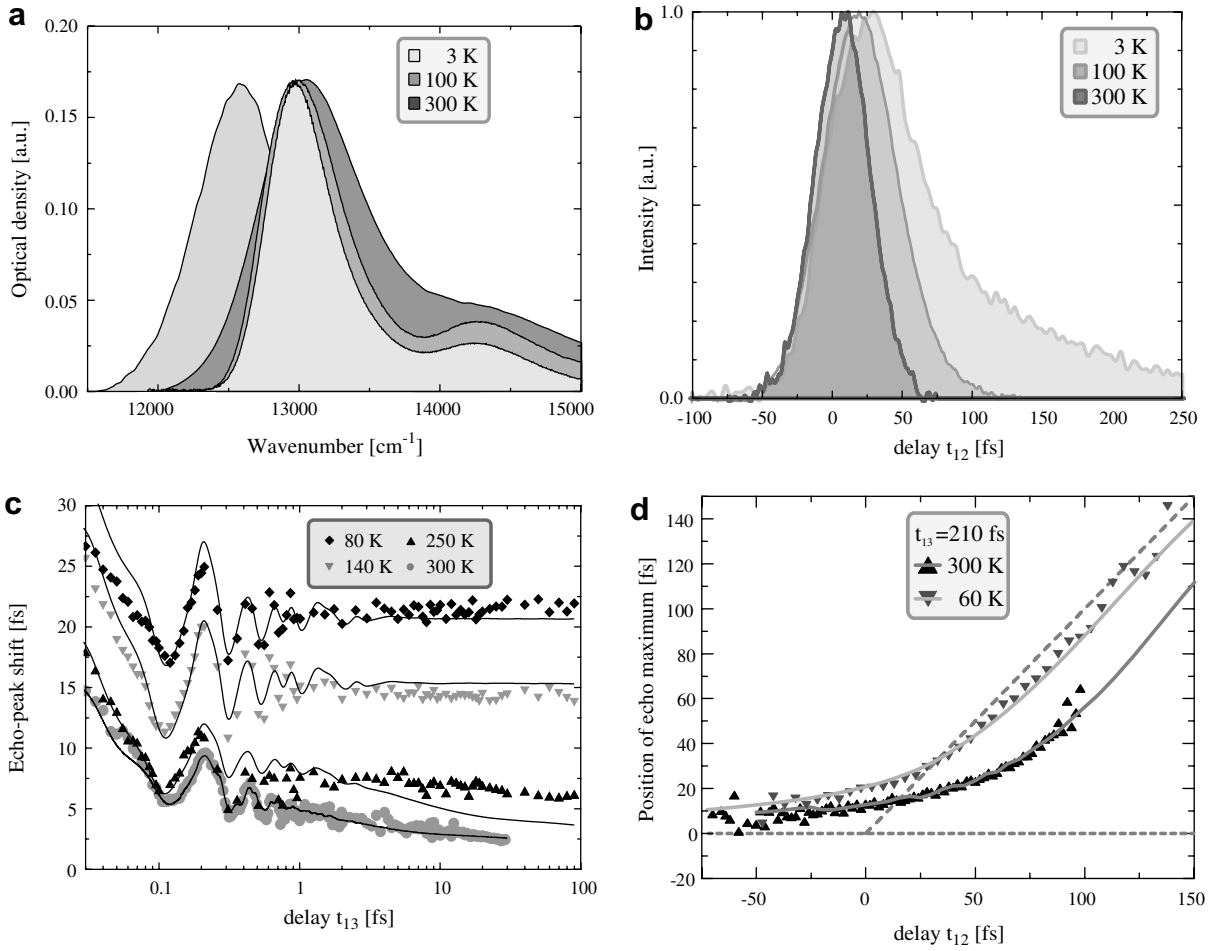

Fig. 3. An overview of the main experiments. (a) The absorption spectrum of DTTCI (right), and the fluorescence at 300 K (left). (b) Time-integrated 3PE scans for $t_{13} = 210$ fs. (c) The 3PEPS signal (symbols) at different temperatures and corresponding simulations (solid lines). (d) The position of the time-resolved echo maxima as a function of t_{12} (symbols) as compared to the full-scale simulations of the positions of these maxima (solid curves) at two representative temperatures.

prominent 150 cm^{-1} mode is almost in its first recurrence (the period is ~220 fs). Second, by a coincidence the 485 cm^{-1} mode is in its third recurrence (the period ~70 fs). Third, the amplitude of the 380 cm^{-1} mode is negligibly small as compared to the other two and therefore its influence is minimized. We will use the 210 fs waiting time in a number of heterodyne-detected experiments to suppress intramolecular vibrational involvement that masks the true solvent dynamics.

Finally, in Fig. 3d the position of the maximum of the HDPE signal is displayed at two different temperatures. In the HDPE experiment, the echo field is heterodyned by a fourth pulse, the local oscillator [31]. By scanning the delay between the last two pulses (t_{34}) for a set of fixed timings of the first two (t_{12}), time-resolved interferometric echo profiles are obtained. For extracting information regarding the homogeneous *vs.* inhomogeneous contributions to the line broadening, the position of the echo maximum has proven to be instructive [31]. For instance, in the framework of the Bloch model [76], the echo maximum peaks at

$$t_{34}^{\max} = t_{12} - \frac{\left(T_2^{\text{inhom}}\right)^2}{T_2}, \tag{19}$$

where T_2^{inhom} and T_2 are the inhomogeneous and homogeneous phase relaxation times, respectively, which can be obtained from the graph presented by Eq. (19). If the line broadening is perfectly static, the time-resolved profile peaks at $t_{34} = t_{12}$ at all times that $t_{12} > 0$. At the other extreme, a totally homogeneous system, profiles always peak at $t_{34} = 0$ fs. In the more sophisticated models of solvent dynamics [30], a relation similar to Eq. (19) also holds although the interpretation of the relaxation times becomes somewhat different [31].

From a fleeting glance at Fig. 3d one could immediately conclude that the plot of the time-resolved echo maximum position follows Eq. (19) reasonably well. From this relation one infers that the estimated dephasing time at 60 K is $T_2 \cong 60$ fs as discussed in more detail in the next sections. Furthermore, if one compares the widths and heights of these traces (not shown) it becomes evident that the transient echo signal broadens with decreasing temperature,

and peaks at a later time. The former corresponds to the narrowing of the absorption spectra as the temperature lowers (Fig. 3a), while the latter indicates their increased inhomogeneity which, of course, can not be directly deduced from the spectra.

4.2. Room-temperature data

In this section, we outline the procedures according to which different experimental data sets were processed. As a starting point, the room-temperature data are used, as much is known for the dye DTTCI dissolved in ethylene glycol from the work by de Boeij where 8 MBO modes were applied to describe the dynamics [31,67,68,75]. The characteristic properties of the EtOH/PD mixture are quite similar to those of ethylene glycol making this the perfect choice for a reference. In the next section, temperature variations of the 8 MBO mode parameters will be introduced to explain the temperature-dependent data.

All of the above experiments reflect particular aspects of the SD associated with the system-bath dynamics. For instance, the absorption and emission spectra are indicative of the overall static coupling strength parameter $\langle \Delta^2 \rangle$ and the total reorganization energy λ. The 2PE and 3PE signals are mostly susceptible to the slow parts of the correlation function while the longitudinal 3PE decay is especially useful to determine the low-frequency intramolecular modes. Alternatively, as explained above, the 3PEPS trace bears great resemblance to the overall correlation function of the energy gap, except for the shortest timescales. In turn, the fast part of the correlation function is best determined through analysis of the time-resolved HDPE traces, as indicated above.

Therefore, all the results at all temperatures from all these techniques have to be taken into account when simulating the temperature dependence of the solute–solvent correlation function or SD in the framework of the MBO model. The iterative numerical procedure that is needed to calculate the correlation function and the corresponding spectral density in this manner was described earlier [31,67,68]. It involves the simultaneous fitting of all spectra, integrated echo traces and transient echo profiles with the results from the calculations. Improvements in computer technology and optimizations of the algorithms used in the calculations have made it possible to perform these calculations on a small cluster of 10 ordinary off-the-shelf desktop PC's.

The calculations of the transient third-order polarization $P^{(3)}(t)$ were performed through the threefold integration of the complete expressions of Eq. (7) and the nonlinear response functions. The actual pulse shapes were taken into account and all possible pulse permutations were incorporated in the computations. After the non-linear polarization was obtained, the simulated signals of the respective experiments were calculated using the appropriate expressions given by Eqs. (17) and (18).

The contributions to the line broadening functions $g(t)$ were, depending on the nature of the mode under consideration, either evaluated directly, whenever an exact expression of this function was available (see Refs. [77,63]) or through numerical integration of the corresponding part of the spectral density. To do this, Eqs. (9)–(11) were rewritten as

$$\mathrm{Re}[g(t)] = \frac{1}{\pi}\int_0^\infty C(\omega)\coth\left[\frac{\hbar\omega}{2k_\mathrm{B}T}\right]\frac{1-\cos[\omega t]}{\omega^2}\,\mathrm{d}\omega \tag{20}$$

and

$$\mathrm{Im}[g(t)] = -\lambda t + \frac{1}{\pi}\int_0^\infty \frac{C(\omega)}{\omega^2}\sin[\omega t]\,\mathrm{d}\omega. \tag{21}$$

In this way the line broadening function can be evaluated numerically by calculating only two single integrals. At room temperature the data were simulated with the set of oscillators outlined in the corresponding column of Table 1.

In earlier work [31], the fastest initial decay was modeled with a quasi-continuum of undamped bath modes with a GSD (see Eq. (16)). For reasons that are discussed in the following sections both the fast intramolecular mode and the inertial solvent mode are modeled here by a single correlation function:

$$M(t) = \frac{\Delta_0^2}{\tau_0}\exp\left[-\frac{t^2}{\tau_0^2}\right]. \tag{22}$$

This Gaussian correlation function (GCF) is associated with the following expression for the corresponding SD $C(\omega)$:

$$C(\omega) = \frac{\Delta_0^2\lambda\omega}{\sqrt{\pi}}\exp\left[-\frac{\omega^2\tau_0^2}{4}\right]. \tag{23}$$

Besides the fast component to the correlation function, the optical transition of DTTCI is coupled to three distinct intramolecular vibrational modes modeled with UBO's (see Eq. (12)). These modes model the periodical recurrences of the observed optical coherence.

Further on, the correlation function decays on three picosecond time scales (sometimes masked by the quantum beats) that reflect collective (diffusional) solvent motions. This part of the decay is modeled by means of three SOBO's (see Eq. (14)). A final extra SOBO with a decay time effectively set to infinity ($\geqslant$1 ns) was used to model the residual inhomogeneity that was invariably found in the response of viscous liquids.

Figs. 3–7 outline the results of simulations using the above parameters and expressions. They demonstrate that the set of parameters from Table 1 can be used to describe all room-temperature experiments adequately.

Fig. 4 displays the emission and absorption spectra at room temperature. Note that the part of the DTTCI absorption spectrum around 14,200 cm^{-1} that is due to excited modes of the conjugated rings of the dye has been largely subtracted to facilitate the comparison of the experimental and simulated data. The calculated spectra fit the

Table 1
The temperature dependence of the fitting parameters of the harmonic modes used to simulate the optical response of DTTCI in EtOH/PD

			Temperature (K)					MBO
			300	250	150	100	3	
Ultrafast mode								
Gaussian decay (GCF)	$\Delta_0 = 850\ cm^{-1}$	τ_0	20 fs	30 fs	80 fs	125 fs	315 fs	No
Intramolecular modes								
Vibrational modes (UBO)	$\omega_1 = 150\ cm^{-1}$	Δ_1	$127\ cm^{-1}$	$117\ cm^{-1}$	$95\ cm^{-1}$	$84\ cm^{-1}$	$74\ cm^{-1}$	Yes
	$\lambda_1 = 37\ cm^{-1}$	γ_1^{-1}	150 fs	182 fs	317 fs	317 fs	317 fs	–
	$\omega_2 = 380\ cm^{-1}$	Δ_2	$43\ cm^{-1}$	$41\ cm^{-1}$	$37\ cm^{-1}$	$37\ cm^{-1}$	$36\ cm^{-1}$	Yes
	$\lambda_2 = 3.5\ cm^{-1}$	γ_2^{-1}	500 fs	600 fs	1 ps	1 ps	1 ps	–
	$\omega_3 = 485\ cm^{-1}$	Δ_3	$81\ cm^{-1}$	$78\ cm^{-1}$	$74\ cm^{-1}$	$73\ cm^{-1}$	$73\ cm^{-1}$	Yes
	$\lambda_3 = 11\ cm^{-1}$	γ_3^{-1}	670 fs	800 fs	1.3 ps	1.3 ps	1.3 ps	–
Solvent modes								
Strongly overdamped modes (SOBO)	$\lambda_5 = 20\ cm^{-1}$	Δ_5	$91\ cm^{-1}$	$83\ cm^{-1}$	$65\ cm^{-1}$	$65\ cm^{-1}$	$65\ cm^{-1}$	Yes[a]
		Λ_5^{-1}	0.5 ps	0.75 ps	>1 ns	>1 ns	>1 ns	–
	$\lambda_6 = 54\ cm^{-1}$	Δ_6	$150\ cm^{-1}$	$137\ cm^{-1}$	$106\ cm^{-1}$	$106\ cm^{-1}$	$106\ cm^{-1}$	Yes[a]
		Λ_6^{-1}	2.5 ps	3.75 ps	>1 ns	>1 ns	>1 ns	–
	$\lambda_7 = 39\ cm^{-1}$	Δ_7	$128\ cm^{-1}$	$116\ cm^{-1}$	$90\ cm^{-1}$	$90\ cm^{-1}$	$90\ cm^{-1}$	Yes[a]
		Λ_7^{-1}	100 ps	150 ps	>1 ns	>1 ns	>1 ns	–
	$\lambda_8 = 46\ cm^{-1}$	Δ_8	$139\ cm^{-1}$	$126\ cm^{-1}$	$98\ cm^{-1}$	$98\ cm^{-1}$	$98\ cm^{-1}$	Yes[a]
		Λ_8^{-1}	>1 ns	>1 ns	>1 ns	>1 ns	>1 ns	–

The MBO-column indicates whether or not the temperature dependence of a particular parameter follows directly from the MBO mode (see text for discussion).
[a] Only above the glass transition.

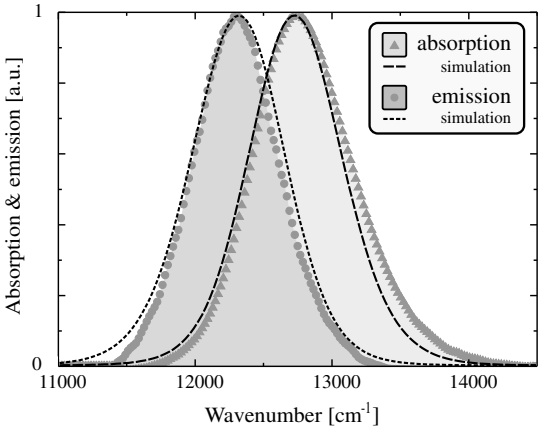

Fig. 4. Absorption and emission spectra at 300 K and the results of the corresponding simulations. The absorption due to ring modes at 14,000 cm^{-1} has been subtracted from the overall spectrum (see text for details).

data very well, except for the small offset on the red side of the emission spectrum. This is caused by the limited number of vibrational modes that are explicitly considered.

The quality of the modeling of 3PE traces can be judged from Fig. 5a. The simulations of longitudinal 3PE profiles (Fig. 5b) show that the quantum beats that are modeled by the three UBO's, are reproduced perfectly, as well as recurrences in the 3PEPS signal (Fig. 6).

Next, a typical time-resolved trace and the corresponding calculations are shown in Fig. 7a. The maximum heights of a series of these traces is compared with the amplitude of the 3PE in Fig. 7b, and shows that the square root of the time-integrated signal matches the heights of the transient echoes.

In Fig. 3d the position of the maximum extracted from a fit of the transients with a Gaussian profile is plotted as a function of the coherence time. Fig. 3d confirms that the calculations match the experimental data closely which means that the parameter set from Table 1 satisfactorily describes both the fast and slow parts of the correlation functions at room temperature. The plots of the maxima at other temperatures will be discussed in the next section of this paper.

All the aforementioned shows that all experiments at room temperature can be reproduced reasonably well with the parameter set presented in Table 1. At first sight an optimization space spanned by nearly 30 free parameters might seem rather excessive. However, it is important to realize that not all these factors are free to take any value. For example, the amplitude Δ_i of each mode is related to the reorganization energy λ_i associated with that mode through the equations outlined above. Although adding more BO modes would of course improve the agreement between experiment and simulation, it is not possible to describe the data accurately with fewer oscillators. The fast initial 3PEPS decay shows clear evidence of two components, and the longitudinal echo traces necessitate the use of at least three UBO's. The diffusive solvent modes are determined by three SOBO's.

Now that the room-temperature data are described adequately by the current set of BO's, we verify how these oscillators can be used to describe the data at different temperatures.

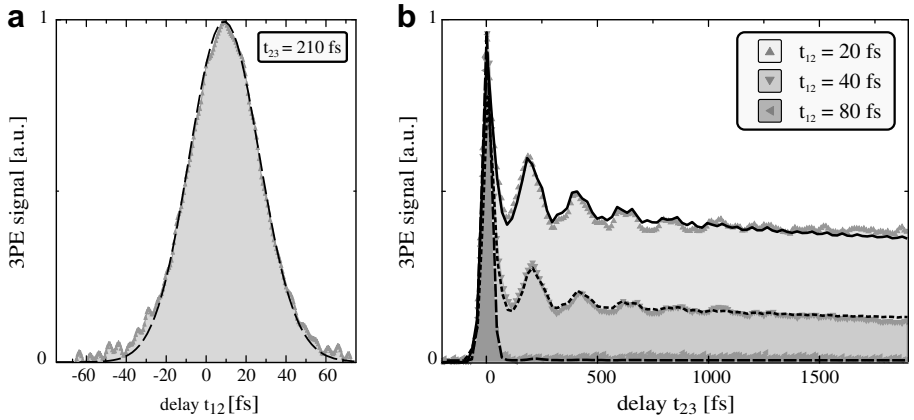

Fig. 5. (a) A typical 3PE trace as used in the determination of the 3PEPS at 300 K. The dashed line shows the simulated echo trace. (b) The longitudinal 3PE at three coherence times t_{12} at room temperature. Again, the black lines, solid, short dashed and long dashed, show the simulations of these experiments.

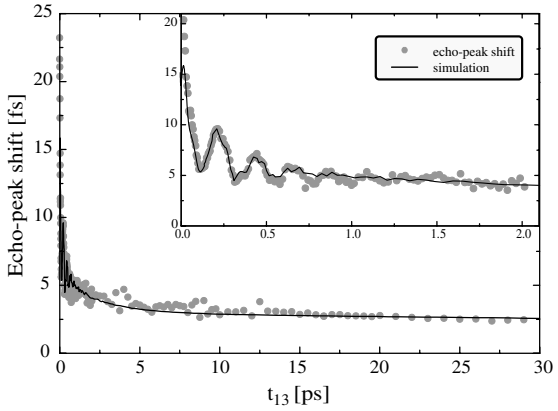

Fig. 6. The 3PEPS signal of DTTCI in PD-EtOH at room temperature and the calculated peak shift trace. The inset shows the short waiting time data.

4.3. Temperature-dependent data

The SD is the key quantity in modeling the system-bath interactions. In a first approach it is supposed not to be dependent on temperature with temperature effects still incorporated in the MBO model through the Boltzmann term in Eq. (20). On the same footing the parameters of the different types of modes depend on temperature. For instance, for an UBO the amplitude can be calculated from the associated reorganization energy and the temperature as follows from Eq. (13). If the HTL holds, the amplitude of the frequency excursions associated with a SOBO depend on temperature through Eq. (15). These temperature dependencies are incorporated in the line broadening function $g(t)$ through the correlation functions $M'(t)$ and $M''(t)$ (see Eqs. (9)–(11)). It should be noted that the modes associated with the GCF cannot obey the HTL. At room temperature, modes with the correlation time faster then ~15 fs do not satisfy this limit, at 30 K the HTL no longer holds for modes faster than ~150 fs and at 3 K even the quickest diffusional mode might not meet the constraints of the HTL.

Even so, if the 300 K parameter set is considered to describe a temperature-independent SD, the model is still capable of accommodating temperature variations. How-

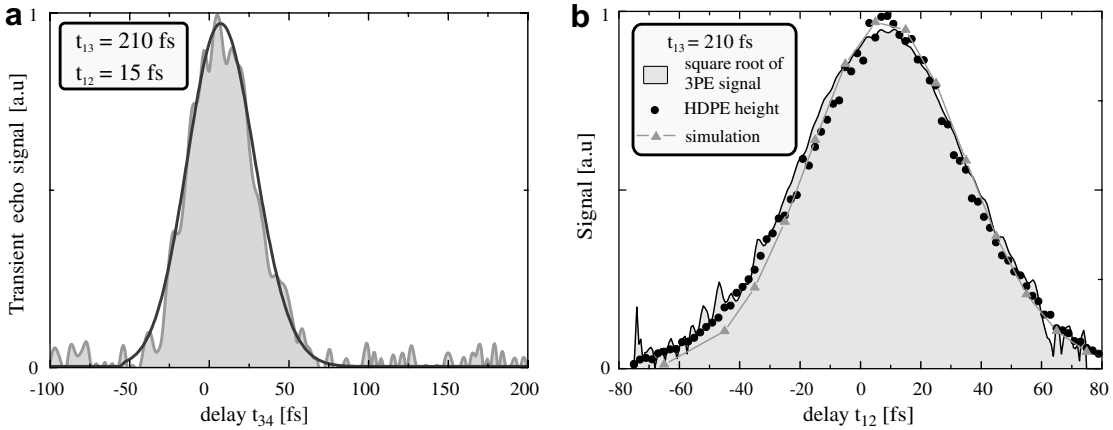

Fig. 7. (a) A typical filtered HDPE trace at room temperature and the corresponding simulated transient echo trace. (b) A comparison of the amplitude of the 3PE with the height of HDPE traces and the transient echo simulations.

ever, it is not likely that the SD remains unchanged over the whole temperature range from 300 to 3 K, especially since this range includes a phase transition. Consequently, some additional temperature dependence of the SD needs to be incorporated in a model that makes physical sense, while varying as few BO parameters as little as possible. Furthermore, such an approach should explain all experiments within the confines of the MBO model.

In the following, the outcomes of several decisive experiments are presented at several temperatures. In order to establish the need for a SD that depends on the temperature, some of these experiments are compared both to calculations that were based on a temperature-dependent and a temperature-independent SD.

Close inspection of experimental data at various temperatures shows that the most apparent temperature-dependent feature is the damping constant of the quantum beats as seen in longitudinal echo decays (Fig. 8) and 3PEPS plots (Fig. 3c). When the longitudinal 3PE plots are fitted with the decaying oscillatory functions, the behavior of especially the damping factors γ_i of the 150 cm^{-1} mode shows significant temperature dependence (Fig. 9). Below the glass transition temperature the decrease of the damping parameter comes to an end. In fact, this slowing of the damping of the intramolecular vibrational modes is the most straightforward observation of the glass transition upon inspection of the individual experiments.

The data in Fig. 9 can be described by the following relation:

$$\gamma_i = \begin{cases} \alpha\gamma_{\text{room}} \frac{T-T_g}{T_{\text{room}}-T_g} + (1-\alpha)\gamma_{\text{room}} & \text{for } T \geqslant T_g, \\ (1-\alpha)\gamma_{\text{room}} & \text{for } T < T_g. \end{cases} \quad (24)$$

Here γ_{room} is the value of γ_i at room temperature T_{room}, and $0 \leqslant \alpha \leqslant 1$. In a global analysis, at the glass point the damping is typically halved with respect to room temperature, and becomes temperature independent below T_g. It is reasonable to assume that when the bath dynamics slow down, the vibrational energy of the chromophore dissipates slower. However, the particular choice for a linear temperature dependence is made on solely phenomenological grounds.

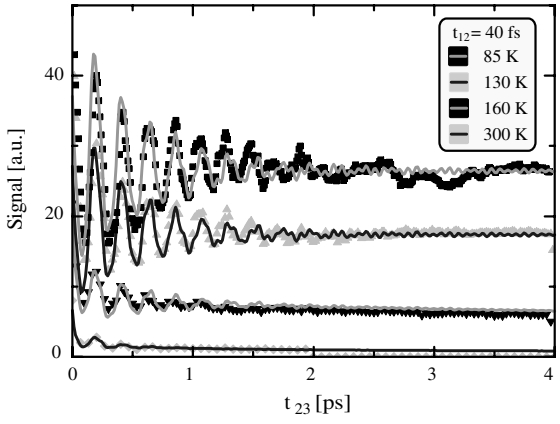

Fig. 8. The longitudinal 3PE traces at $t_{12} = 40$ fs at several temperatures (symbols) and the corresponding calculations (lines) according to Table 1.

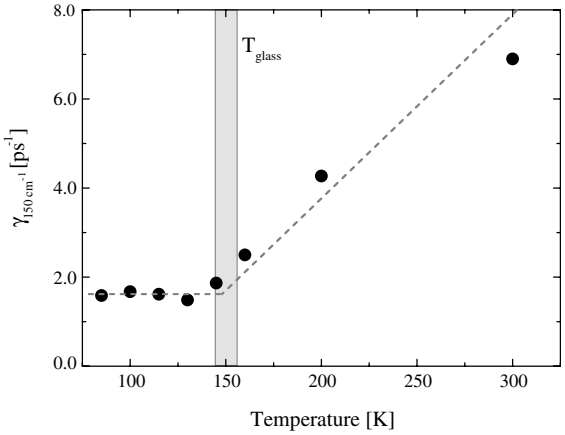

Fig. 9. The temperature dependence of the damping of the 150 cm^{-1} vibrational mode of DTTCI in EtOH/Pd shows the effect of the glass transition (grey bar) on the vibrational mode, when only changes to the vibrational modes are considered. The dotted line is a fit to the data with Eq. (24).

At the same time, when considering the solvent modes, it is reasonable to expect that diffusion vanishes below the glass temperature. Therefore, a temperature dependence was introduced for SOBO's, that is consistent with the freezing out of solvent diffusional modes. The conjecture is a scheme in which all modes show the temperature dependence through the relations within the MBO model as outlined above while the diffusional and dissipation times are sensitive to the temperature. The data were adequately described at all temperatures below T_g by setting the parameters of the ith SOBO as follows: Δ_i^2 was set to its value at the glass temperature according to Eq. (15), and the correlation time Λ_i^{-1} was set to infinity (>1 ns). Therefore, the strongly overdamped solvent modes were considered as contributing to the overall static inhomogeneity below the phase transition temperature. Above the glass temperature, similarly to Eq. (24), Λ_i was set to linearly increase from zero to its value at room temperature:

$$\Lambda_i = \Lambda_{\text{room}} \frac{T - T_g}{T_{\text{room}} - T_g}. \quad (25)$$

The behavior expressed in Eq. (25) is inspired by the Vogel–Fulcher equation describing non-Arrhenius relaxation in glass-forming liquids [11,12]. Here the divergence temperature of the Vogel–Fulcher equation is set equal to the glass temperature.

So far, the proposed scenario is simple and physically appealing, since it only implies the slowing down of solvent modes and vibrational energy dissipation as the glass transition is approached. Unfortunately, it yields too little inhomogeneity at temperatures well below T_g which results in strongly underestimated values of echo-peak shift values. This is illustrated by Fig. 10a that shows the difference between the calculated 3PEPS using the parameters

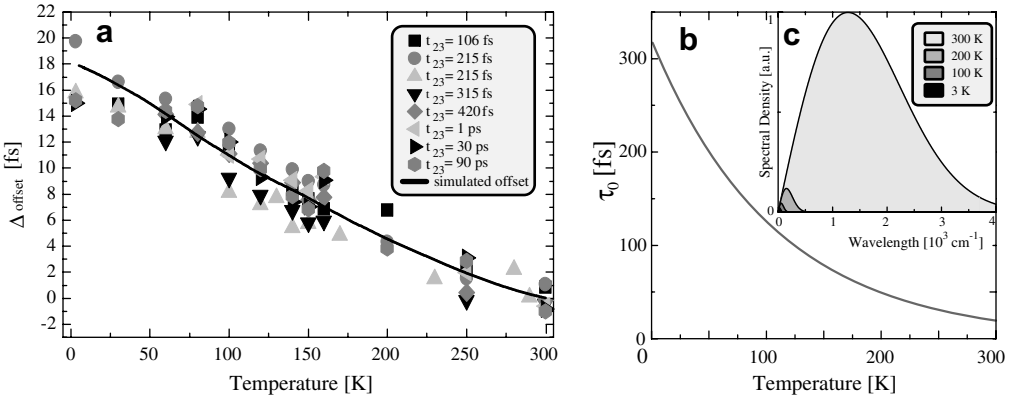

Fig. 10. (a) The difference between the experimental and simulated echo-peak shift data at several waiting times without considering the temperature dependence of the fast GCF mode (symbols). The solid line shows the averaged difference between the simulation with and without this temperature dependence. (b) The proposed temperature dependence of the characteristic time τ_0 of the GCF mode. (c) The spectral density associated with the temperature-dependent GCF mode.

temperature variation as introduced above by Eqs. (24) and (25), and the experimental 3PEPS data at several waiting times as a function of temperature. The parameters of the fast mode were set to match the data at room temperature. Clearly, an offset exists between the calculated echo-peak shift and its experimental values which is virtually independent on the waiting time. This indicates that the correlation time of the fastest MBO mode, introduced in the previous section by Eq. (22) must also vary with temperature:

$$M(t) = \frac{\Delta_0^2}{\tau_0(T)} \exp\left[-\frac{t^2}{\tau_0(T)^2}\right]. \tag{26}$$

By increasing the characteristic timescale τ_0 of this mode with decreasing temperature, the echo decay slows enough to let the simulated 3PEPS coincide with the experimental values. As the 3PEPS does not vary linearly with the correlation time of this fast mode, a simple linear temperature dependence is not capable explaining the experimental results in a satisfactorily manner. In simulation the temperature dependence of the characteristic time was chosen *ad hoc* to be exponential:

$$\tau_0 = \alpha_1 \exp\left[-\frac{T}{\alpha_0}\right]. \tag{27}$$

Note that other parameterization functions, in particular, involving both time and amplitude could have been used as well.

The dependence of the correlation time on temperature expressed by Eq. (27) is shown in Fig. 10b while the contribution of the mode presented described by Eq. (26) to the overall SD is depicted in Fig. 10c. These values were obtained by setting $\alpha_0 = 107$ K and $\alpha_1 = 320$ fs as follows from the room-temperature data. The amplitude Δ_0 of the mode was taken to be temperature independent. Since at all temperatures the characteristic time of the GCF is still shorter than those of any other modes, the contribution of the fast mode varies as $\propto \Delta^2/\tau_0$. Therefore, with the temperature decrease, first, the SD of the bath fluctuations decreases in amplitude, and second, it spans a narrower spectral region (Fig. 10c). As the fast intramolecular mode is associated with vibrational dephasing and/or inertial solvent motion, both trends meet the intuitive expectations. Nonetheless, the implied temperature dependence does not follow automatically from the MBO model, most probably, due to the breakdown of the assumption of linear coupling to the vibronic manifold.

The difference between the simulated echo-peak shift data without and with the temperature-dependent GCF is represented by the solid line in Fig. 10a. This shows that the chosen temperature dependence given by Eq. (27) is effective in eliminating the last remaining difference between the simulated 3PEPS traces and the experimental data. After this final tweak the scenario, with all relevant parameters outlined in Table 1, yields good results. Of course, having more parameters that vary more freely with temperature can improve the match between experimental data and the calculations, but the proposed scenario is the simplest of all tested arrangements.

The first evidence of the ability of this scenario to describe the data is with the temperature dependence of the absorption spectra (Fig. 11). To emphasize the need for a temperature-dependent SD to accurately simulate the data, the absorption spectra were also calculated with a temperature-independent SD (the grey triangles). The spectra can be reproduced over the complete temperature range reasonably well if the correlation time of the GCF obeys Eq. (27). In contrast, with the temperature-independent SD most of the broadening is missed at low temperatures.

The longitudinal echo traces are well reproduced, too, as demonstrated in Fig. 8. These traces especially reinforce the necessity of making the damping of the vibrational modes temperature dependent. The temperature dependence of the parameters that make up the UBO modes is characterized accurately. Close inspection shows that although there

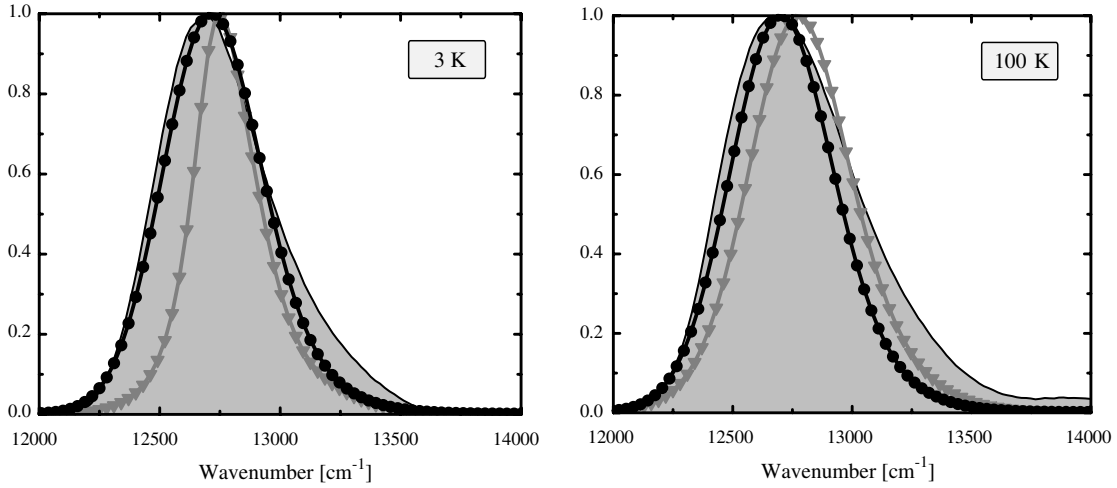

Fig. 11. The absorption spectra of DTTCI in EtOH/PD at two different temperatures (solid lines) and the calculations with the parameters in Table 1 (black circles). In all absorption spectra the ring modes with at 14,000 cm^{-1} were subtracted. The grey triangles indicate the absorption spectrum simulated with a temperature-independent SD.

is some room for improvement of the fits, the data do not yield evidence enough for more complicated schemes than the one described in Eqs. (24)–(27).

The 3PE echo profiles are reproduced similarly well at all waiting times and temperatures (Fig. 12) except for short waiting times (<1 ps) at very low temperatures (<5 K). Since at these times and temperatures the HTL no longer holds, the mismatch between experiment and simulation in the last panel of Fig. 12 is to be expected. Otherwise the echo width and echo position are reproduced accurately. Again, the lack of temperature dependence of the fast mode would result in too narrow echo signals at temperature below 300 K. In addition, the maxima of the echoes (i.e. echo-peak shifts) would have been strongly underestimated.

The echo-peak shift data are reproduced reasonably well at the various temperatures which also demonstrated the effectiveness of the proposed scenario. Fig. 3c shows evidence of the separation of the fast intramolecular modes not being sensitive to the glass transition, and the slow diffusive solvent modes that are susceptible to that. Although at some temperatures the experimental asymptotic long-time echo-peak shift is not perfectly accounted for in the simulations, the trends of the values are replicated quite well. The mismatch between experiment and simulations is too small to warrant further refinement of the proposed temperature dependence.

Fig. 13 plots the detailed temperature-dependent data of the 3PEPS at two waiting times that correspond to the first vibrational recurrence at 210 fs and almost full relaxation at room temperature at 100 ps. The temperature dependence of these echo-peak shifts is emulated by the simulations. Interestingly enough, the short time echo-peak shift shows little evidence of a discontinuity at the phase transition around 150 K. Only at long waiting times the glass to liquid transition is visible in the experimental 3PEPS results. This is reasonable to expect, since the fast modes are not sensitive to this change in the bath dynamics, and the solvent modes are too slow to influence the echo-peak shift at the 210 fs waiting time. At even lower temperatures, as the system becomes more inhomogeneous, the solvent relaxation nearly vanishes altogether. The offset between

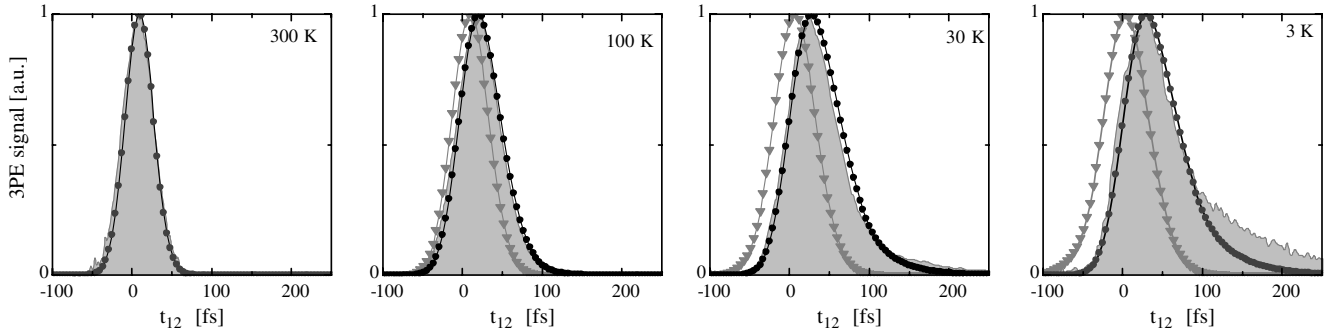

Fig. 12. Typical 3PE traces at various temperatures (solid lines). The waiting time for these traces is $t_{13} = 210$ fs. The black circles indicate the simulations with a temperature-dependent SD and the grey triangles simulations with a temperature-independent SD.

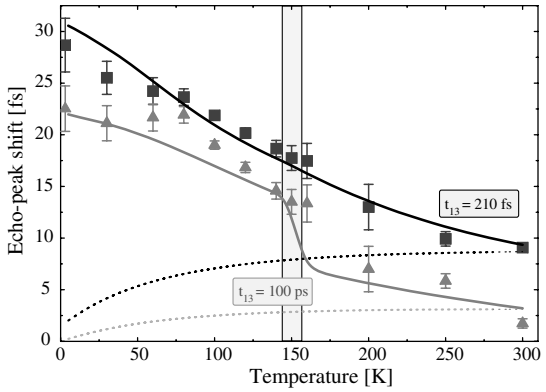

Fig. 13. The temperature dependence of the echo-peak shift at waiting times $t_{13} = 210$ fs (black symbols) and $t_{13} = 100$ ps (grey symbols). The solid lines are simulations of the experimental data using the scenario outlined in the text. The dotted lines are simulations assuming a fixed temperature-independent SD. The glass temperature T_g is indicated by the grey bar.

these two data sets at temperatures below the glass transition originates mainly from the vibrational relaxation of the 150 cm^{-1} intramolecular mode, and the temperature-dependent terms in Eq. (20).

Finally, Fig. 14 shows the temperature dependence of the HDPE data. Here, positions of the maxima of transient echo traces are depicted at various temperatures and two waiting times. As with the room-temperature data, the maxima of the Gaussian fits to the transient echo traces are plotted as a function of the coherence time. The positions of the maxima also compare well with the theoretical predictions based on the proposed scenario for the temperature dependence of the BO parameters. Decreasing the temperature and decreasing the waiting time have a similar effect on the plots: the time-resolved echo peaks closer to the delay between the first excitation pulses (diagonal lines).

Fig. 15 summarizes the temperature dependence of the maximum of several slices of these echo maximum profiles at a waiting time of $t_w = 210$ fs at different temperatures. It is immediately clear that the system grows to be more static at lower temperatures. From 300 K to the glass temperature at 150 K, the dynamics slow down in a linear fashion. Then, deceleration of the solvent dynamics seemingly comes to a halt around the glass temperature. At longer coherence times at low temperatures the maxima are positioned at nearly the same delay as the corresponding coherence time, indicating a primarily static and inhomogeneous character of the dephasing dynamics. Note that the glass transition is clearly discernable in the experimental HDPE data even at the 210 fs waiting time (Fig. 15), as opposed to the temperature-dependent 3PEPS data (Fig. 13). The origin of this phenomenon originated from the breakdown of the linear dependence of the correlation function on the echo-peak shift under overwhelming inhomogeneity of the optical transition [31,55,56,67–69], will be addressed in detail elsewhere [77].

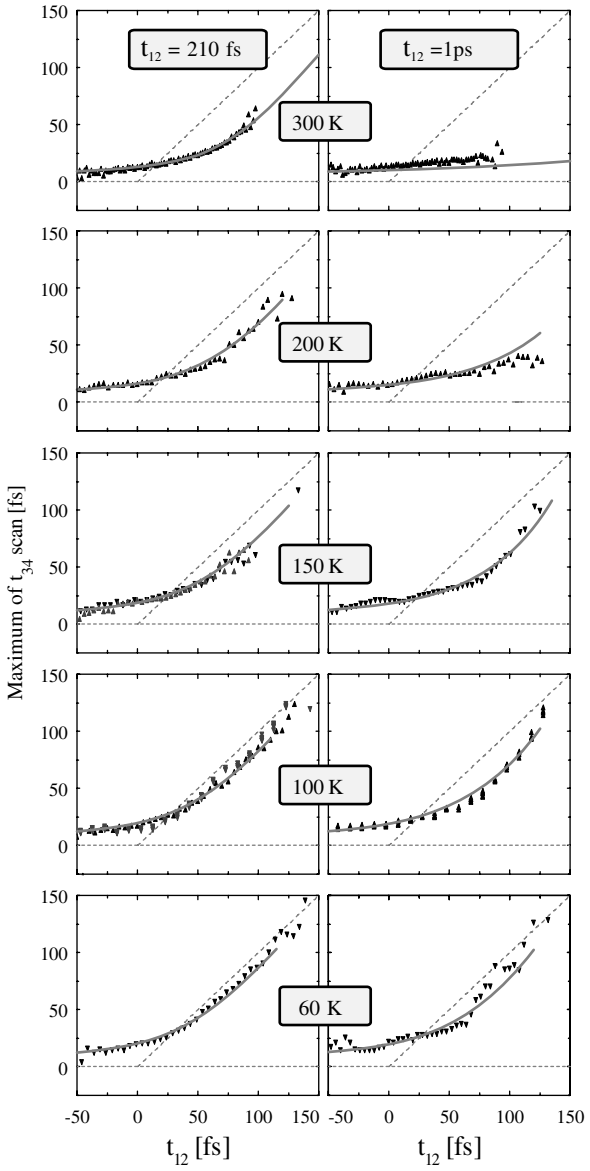

Fig. 14. The maxima of transient echo traces at various temperatures at two waiting times (black triangles) with the corresponding calculations (grey lines). The dotted lines indicate the expected experimental outcome in case of a perfectly homogeneously (horizontal line) and inhomogeneously (diagonal line) broadened system.

5. Discussion

The scenario for the temperature dependence of the spectral density introduced in the previous section has been used to successfully simulate the experimental data. The choices implemented in this scenario are made mainly on phenomenological grounds. The feasibility and credibility of these grounds are discussed in further detail in this section.

Within the MBO model, when still taking the shape of the spectral density as temperature independent, the amplitude of the frequency fluctuations Δ_i are assumed to depend on temperature while the associated reorganization

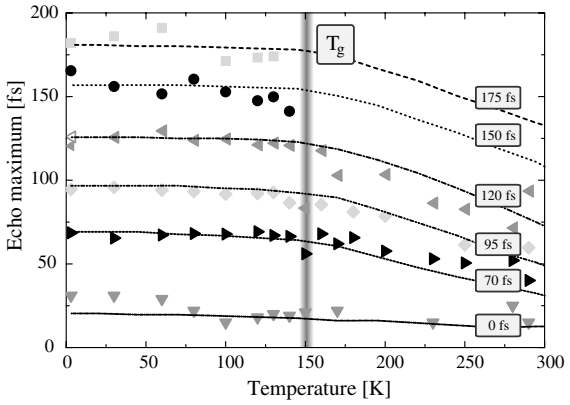

Fig. 15. The position of the maximum of the time-resolved echo profile at different coherence times t_{12} as a function of temperature (symbols) and the corresponding calculations (lines). The waiting time was set at 210 fs.

energy λ_i is a constant. The justification of this lies in the fact that in the framework of the MBO model the reorganization energy is directly connected with the displacement d between the ground and excited-state potential energy surfaces of the chromophores along the generalized solvent coordinate [78]. Also, the absorption spectra exhibit some narrowing of their widths at lower temperatures which is consistent with decreasing of the frequency fluctuations amplitude. Finally, the argument that the Stokes shift (that is directly related to the reorganization energy) decreases with decreasing temperature, is refuted by noticing that the time scale at which the solvent reorganization occurs, at low temperatures becomes much longer than the excited-state lifetime. Therefore, the population relaxes long before the solvent has a chance to get reorganized and therefore to produce the frequency-shifted fluorescence.

The temperature dependence of the remaining BO parameters (i.e., reorganization energy λ_i, damping γ_i and frequency ω_i) is rarely discussed in current literature. Gu et al. remarked that in their full quantum mechanical treatment of an electronic excitation linearly coupled to multiple passively damped harmonic oscillators, the damping coefficient should be regarded as a function of temperature and frequency $\gamma_i = \gamma_i(T, \omega)$ [79]. They also noted that the specific temperature dependence is especially relevant if one considers the effects of a phase transition of the solvent. The ultimate cause of the damping of the UBO modes is the interaction of the optical system with the environmental solvent shells, and one would expect a large effect on the damping from the fluid's viscosity. Therefore, the authors concluded that the temperature dependence of γ_i is determined by the specific physical origin of the damping of the mode under consideration. For these reasons in the last column of Table 1 the parameters that vary with temperature purely following Eqs. (13) and (15) are indicated as following directly from the MBO model, whereas the temperature dependence of the damping parameters γ_i and Λ_i is not included in the model.

The damping of the slow intramolecular modes discussed here, is determined by how quickly the vibrational energy dissipates into the surrounding solvent. In the absence of a solid theoretical framework the choice for linear variation of the damping of the underdamped oscillator with temperature follows readily from the experimental longitudinal 3PE data, as can be seen in Fig. 9. The damping rates are relatively moderate, at the subpicosecond time scale. The slower relaxation processes, related to structural equilibration, should correlate well with the Stokes–Einstein equation that provides the relation between the self-diffusion coefficient D and the viscosity η [80]:

$$D(\eta) = \frac{kT}{6\pi\eta r}. \tag{28}$$

A similar relation exists for the rotational reorientation time, the Debye–Einstein relation [80]. Therefore, as the diffusion coefficient decreases linearly with temperature, the microscopic structural relaxation times will increase in a similar fashion. It has been established that this concept of evaluating hydrodynamic and thermodynamic functions of the solvent can be used to describe the solute–solvent coupling [81,82]. The linear character of temperature dependence has been observed in Raman spectra of amorphous metal solids [83], and in IR pump–probe studies on the temperature-dependent vibrational relaxation times of carbonyls solutes in various liquids [84,85]. Although this evidence is indirect, it indicates that the linear temperature dependence of the vibrational relaxation in the experiments presented here is reasonably realistic.

The temperature dependence of the inverse correlation time Λ_i of the strongly overdamped modes is established using the same concept of correlated temperature dependencies of relaxation times. As it is reasonable to expect that all diffusive motion disappears at temperatures below the glass transition, this temperature is used as the divergence temperature in a Vogel–Fulcher description [11,12]. This can be regarded as a first-order approach to model non-Arrhenius relaxation in glass-forming liquids. This is also in line with transient-dichroism experiments which have demonstrated a similar correlation with viscosity and temperature [86–94].

The main experimental motivation for the linear temperature dependence of the inverse correlation time Λ_i of the solvent modes above the glass temperature was the temperature dependence of the HDPE traces, as displayed in Fig. 15. The apparent linear temperature dependence of the echo maximum position, especially for longer coherence times, means that the inhomogeneous character of the system increases proportionally as the glass transition is approached (cp. Eq. (19)).

The maximum of the transient echo signal is found by differentiating Eq. (18) with respect to local oscillator time t_{34}, and finding the zero crossing. From this, in a first order approximation the linear dependence of the maximum

position of t_{max} on the inverse correlation time is derived at long coherence times:

$$t_{max} = t_{12} - \frac{\Lambda_i}{\Delta_i^2}. \quad (29)$$

A linear temperature dependence of the diffusive solvent mode parameters is consistent with this result. Another functional form of this temperature dependence will not be consistent with the data because of the connection between the 3PEPS and the HDPE results. Changing the parameters of the strongly overdamped modes to let the simulations match, for instance, the echo-peak shift data will also change the simulated transient echo maximum position.

Whereas the temperature dependence of the parameters of the above modes is in accordance with the physical interpretation of the associated relaxation processes, that of the fastest intramolecular correlation decay is not. The temperature dependence of the modes associated with the GCF does not follow naturally from the interpretation that this correlation decay stems from ultrafast dephasing of the vibronic manifold. The fast inertial solvent contribution found in studies of liquid dynamics in the femtosecond time domain is not necessarily viscosity dependent. Here the amplitude of the GCF was taken to vary exponentially with temperature through the characteristic time τ_0. This functional dependence was chosen on purely phenomenological grounds and also for its simplicity. However, the experimental data can also be described with other functional dependencies with sufficient accuracy.

Summarizing the discussion on the temperature-dependent parameters, all the BO parameters that vary with temperature, do so in a manner that is consistent with the physical origin of the modes that they describe. However, the additional variation of the decay time of the fastest mode is required to match all simulation with all experiments consistently.

6. Conclusions

In this paper the effects of temperature on solvation dynamics have been studied by measuring the optical dephasing of a coherently excited ensemble of chromophores in a liquid/glass surrounding. The solvent, a glass-forming liquid, has been cooled from room temperature down to 3 K, a temperature range that includes the glass transition of this liquid at 150 K. Temperature-dependent optical dephasing in condensed matter has never been studied over a temperature range this wide nor through a phase transition.

The optical dephasing has been studied through the third-order optical polarization by means of two and three-pulse photon echo experiments, echo-peak shift measurements, heterodyned photon echoes, and the linear spectra. The results of all these experiments have been interpreted in terms of the multimode Brownian oscillator model. It was found that a temperature-independent spectral density of states cannot be used to describe the experimental results. However, varying this spectral density in a manner that follows readily from the physical interpretation associated with the various modes, yields excellent results.

Underdamped modes that represent vibrational modes of the chromophore are found to have damping rates that are proportional with temperature down to the glass transition, and temperature independent below that. This reflects slower vibrational energy dissipation at lower temperatures into the bath.

The strongly overdamped modes that are associated with slow diffusional solvent motion also depend on temperature in a nearly linear fashion. The correlation time of these modes increases with decreasing temperature until the glass transition. When all diffusional solvent motion is frozen out, the correlation times become infinitely long. This corresponds well with solidification of the solvent.

Since changing parameters like the damping rate of underdamped modes always changes the spectral density, the MBO model cannot capture the temperature dependence above the glass temperature. Only in a solvent that does not show major changes in its thermodynamic bulk properties, the MBO model does properly account for the temperature dependence of the optical response of the system by only varying the thermal occupation of the bath. This is, for instance, the case in a polymer below its glass transition point [40–42]. However, even then the temperature dependence of the ultrafast intramolecular dephasing is likely to cause problems at lower temperatures.

The description of the ultrafast mode was changed from the spectral distribution of undamped modes used by de Boeij et al. to a Gaussian correlation decay that is associated with a spectral density that goes linearly to zero with the frequency. The SD has to approach zero at the lowest frequencies in this manner in order to have a description that yields reasonable polarization decays. The characteristic time of this decay was found to depend exponentially on temperature.

Having modeled the correlation function by means of one fast mode, three intramolecular underdamped and four strongly damped solvent modes it is possible to simulate all the experiments, including absorption and emission profiles, at all temperatures with a reasonable degree of accuracy. This was done using a limited and closed set of BO parameters that vary with temperature in a way that is expected considering the physics involved.

The solvation dynamics of DTTCI in a PD/EtOH mixture can only be described with a temperature-dependent SD. This is especially true above the glass transition temperature. The slowing down of molecular motion with decreasing temperature is clearly reflected in the characteristics of the corresponding MBO description. Even below the glass transition, when all solvent motion has vanished the SD is somewhat temperature dependent to make the behavior of the inertial ultrafast contributions in the MBO model reflect the optical dephasing.

The 3PEPS results at a waiting time of 210 fs do not show signs of the glass transition because the solvent modes are too slow to have a noticeable effect on the echo-peak shift at that time. This demonstrates the importance of time resolving the echo signal with a heterodyning field. In the HDPE results at the same waiting time, the glass transition is clearly discernible. It underlines the strengths of this technique; the heterodyned data allow for a much better separation of the contributions of the various modes. The HDPE technique can reveal dynamics that would have gone unnoticed in a time-integrated experiment.

From all this it can be concluded that especially time-resolved optical techniques are powerful tools in studying the ins and outs of solvation dynamics. Here it was shown that a PD/EtOH mixture shows large aberrations from Arrhenius behavior, and can therefore be considered a fragile liquid. The temperature dependence of bulk properties such as self-diffusion and viscosity in super-cooled liquids in general is complex, and cannot easily be described by a single relation. Furthermore the temperature dependence in this regime in this solvent was sampled to coarsely to allow detailed comparisons between the temperature dependence of the bath modes and that of bulk properties. However, the measurements did show strong aberrations from Arrhenius temperature dependence and justified the use of an approach that incorporates a divergence temperature.

The difficulty in studying solvation dynamics through optical dephasing lies in the precise characterization of all the contributions to the correlation decay and the subsequent separation of intramolecular modes and solvent modes. The photon echo experiments are also inherently ensemble experiments and therefore not sensitive to the non-ergodic aspects of the glass transition and the solvation dynamics of the super-cooled liquid. It would be naïve to expect the MBO model to describe a system going through dramatic changes with a single static spectral density of states. However, this does not invalidate this model, but it rather shows that when modeling an optical response with a linearly coupled harmonic heat bath the model has to be applied with caution.

Furthermore, the MBO model does not include any difference between the potential energy surfaces of the ground and excited states. If these surfaces are not identical, the energy gap is no longer linearly coupled to the generalized solvation coordinate, and quadratic coupling terms need to be considered as well. This leads to extra dephasing terms that should be taken into account. Possible anharmonicity of the potential energy surfaces is yet another relevant process that leads to the appearance of the non-linear coupling. This is less likely to be important at room temperature as the fast bath dynamics ensure the Gaussian statistics of the fluctuations of the energy gap. However, at temperatures below the glass transition the bath dynamics become far more static, and therefore the averaging of the solvent motions might be less effective making the Gaussian character of the statistics of the collective solvent coordinate is less probable. In either case, the second-order cumulate truncation of the non-linear response functions can not be used. On top of that, the Condon approximation (i.e. independence of the transition dipole moment on the generalized solvation coordinate) becomes questionable as it was pointed out for IR photon echo spectroscopy on liquid water [95]. Fortunately, the impressive progress in computational power allows lifting these approximations thereby directly calculating the non-linear response functions.

Acknowledgements

We are grateful to Shaul Mukamel, Dwayne Miller, Keith Nelson, and Erik Nibbering for many fruitful discussions. The Netherlands Organization for Scientific Research (NWO) is acknowledged for financial support of this work.

Most of all, the authors would like to thank Prof. Dr. Douwe A. Wiersma, to whom this paper is dedicated. Douwe's long-standing interest in the optical properties of condensed matter in general, and glasses in particular, inspired this work. As a result, many of his ideas have been implemented in this paper. It adds to a long line of research that was initiated by Douwe several decades ago [96] (see the epigraph), and to which the authors are proud to contribute. On the inside of the door of Douwe's office hangs a photograph of an oscilloscope screen, with his lab's first ever photon echo signal. It stems from the days when *ultrafast* was still measured in *nano*- rather than *femto*-seconds.

For many years we had the pleasure and privilege to work alongside Douwe who was a great teacher and motivator to us. Discussions in this office always proved to be inspiring because of Douwe's exceptional skill to combine detailed knowledge with a strong focus on the core issues, but, most of all, because of his unbridled enthusiasm. This enthusiasm is applied to not just science but almost any subject else. Douwe takes a genuine interest in the people around him and the things that matter to them. This has contributed to the sense of team spirit that is felt by the (ex)students of the *Ultrafast Laser and Spectroscopy Laboratory* at the Department of Chemistry. And it makes that this lab, despite its mundane setting in the dark basement (attention: *laser radiation!*), feels like home to us.

References

[1] H. Rawson, Properties and Applications of Glass, Elsevier, Amsterdam, 1985.
[2] H. Rawson, Glasses and Their Applications, IOM Communications, Leeds, 1991.
[3] R. Zallen, The Physics of Amorphous Solids, John Wiley & Sons, New York, 1998.
[4] P.W. Anderson, Basic Notions of Condensed Matter Physics, Westview Press, Reading, MA, USA, 1997.
[5] C.A. Angell, J. Phys.: Condens. Matter 12 (2000) 6463.
[6] C.A. Angell, Solid State Ionics 105 (1998) 15.
[7] C.A. Angell, Supercooled Liq. 676 (1997) 14.
[8] W. Kauzmann, Chem. Rev. 43 (1948) 219.

[9] J.H. Gibbs, E.A. DiMarzio, J. Chem. Phys. 28 (1958) 373.
[10] F.H. Stillinger, J. Chem. Phys. 88 (1988) 7818.
[11] H. Vogel, Physik. Z. 22 (1921) 645.
[12] G.S. Fulcher, J. Am. Ceram. Soc. 8 (1925) 339.
[13] C. Hansen, F. Stickel, R. Richert, E.W. Fischer, J. Chem. Phys. 108 (1998) 6408.
[14] C. Hansen et al., J. Chem. Phys. 107 (1997) 1086.
[15] F. Stickel, E.W. Fischer, R. Richert, J. Chem. Phys. 104 (1996) 2043.
[16] F. Stickel, E.W. Fischer, R. Richert, J. Chem. Phys. 102 (1995) 6251.
[17] F. Stickel, E.W. Fischer, A. Schönhals, F. Kremer, Phys. Rev. Lett. 73 (1994) 2936.
[18] K.L. Ngai, Physica A 261 (1998) 36.
[19] U. Bengtzelius, W. Götze, A. Sjölander, J. Phys. C: Solid State Phys. 17 (1984) 5915.
[20] W. Götze, L. Sjögren, Rep. Prog. Phys. 55 (1992) 241.
[21] W. Götze, J. Phys.: Condens. Matter 11 (1999) A1.
[22] E. Leutheusser, Phys. Rev. A 29 (1984) 2765.
[23] G. Adam, J.H. Gibbs, J. Chem. Phys. 43 (1965) 139.
[24] C.A. Angell et al., J. Appl. Phys. 88 (2000) 3113.
[25] H. Frauenfelder et al., Physica D 107 (1997).
[26] S. Sastry, Nature 409 (2001) 164.
[27] S. Sastry, P.G. Debenedetti, F.H. Stillinger, Nature 393 (1998) 554.
[28] H.C. Meijers, D.A. Wiersma, Phys. Rev. Lett. 68 (1992) 381.
[29] H.C. Meijers, D.A. Wiersma, J. Chem. Phys. 101 (1994) 6927.
[30] S. Mukamel, Principles of Nonlinear Optical Spectroscopy, Oxford University Press, New York, 1995.
[31] W.P. de Boeij, M.S. Pshenichnikov, D.A. Wiersma, Annu. Rev. Phys. Chem. 49 (1998) 99.
[32] R.F. Loring, S. Mukamel, Chem. Phys. Lett. 114 (1985) 426.
[33] S. Mukamel, R.F. Loring, J. Opt. Soc. Am. B 3 (1986) 595.
[34] Y.J. Yan, S. Mukamel, J. Chem. Phys. 88 (1988) 5735.
[35] Y.J. Yan, S. Mukamel, J. Phys. Chem. 93 (1989) 6991.
[36] A.M. Weiner, S. de Silvestri, E.P. Ippen, J. Opt. Soc. Am. B 2 (1985).
[37] S. de Silvestri, A.M. Weiner, J.G. Fujimoto, E.P. Ippen, Chem. Phys. Lett. 112 (1984).
[38] C.J. Bardeen, G. Cerullo, C.V. Shank, Chem. Phys. Lett. 280 (1997) 127.
[39] C.J. Bardeen, G. Cerullo, C.V. Shank, Temperature-dependent electronic dephasing of molecules in polymers measured by femtosecond three pulse photon echoes, Ultrafast Phenomena, 1996.
[40] Y. Nagasawa, S.A. Passino, J. Taiha, G.R. Fleming, Femtosecond 3 pulse stimulated photon echo peak shift measurements of organic polymer glass from room temperature to 30 K, Ultrafast Phenomena, 1996.
[41] Y. Nagasawa, Y.Y. Jae, G.R. Fleming, J. Chem. Phys. 109 (1998) 6175.
[42] Y. Nagasawa, Y.Y. Jae, C. Minhaeng, G.R. Fleming, Faraday Discuss. (1997).
[43] Y.G. Vainer et al., J. Lumin. 86 (2000) 265.
[44] Y.G. Vainer et al., J. Chem. Phys. 116 (2002) 8959.
[45] N.V. Gruzdev, E.G. Sil'kis, V.D. Titov, Y.G. Vainer, J. Phys. IV 1 (1991) 439.
[46] N.V. Gruzdev, E.G. Sil'kis, V.D. Titov, Y.G. Vainer, J. Opt. Soc. Am. B 9 (1992) 941.
[47] N.V. Gruzdev, Y.G. Vainer, J. Lumin. 56 (1993) 181.
[48] Y.G. Vainer, N.V. Gruzdev, Opt. Spectrosc. 76 (1994) 232.
[49] T. Elsaesser, W. Kaiser, Annu. Rev. Phys. Chem. 42 (1991) 83.
[50] G. Van der Zwan, J.T. Hynes, J. Phys. Chem. 89 (1985) 4181.
[51] M. Maroncelli, J. Mol. Liq. 57 (1993).
[52] B.M. Ladanyi, R.M. Stratt, J. Phys. Chem. 99 (1995) 2502.
[53] P.V. Kumar, M. Maroncelli, J. Chem. Phys. 103 (1995) 3038.
[54] M. Maroncelli, V.P. Kumar, A. Papazyan, J. Phys. Chem. 97 (1993) 13.
[55] G.R. Fleming, M.H. Cho, Annu. Rev. Phys. Chem. 47 (1996) 109.
[56] S.J. Rosenthal, X. Xie, M. Du, G.R. Fleming, J. Chem. Phys. 95 (2006) 4715.
[57] S. Yoshioka, Y. Miyake, J. Watanabe, S. Kinoshita, J. Lumin. 94 (2001) 771.
[58] S. Kinoshita, Y. Kai, Y. Watanabe, J. Watanabe, J. Lumin. 87 (9) (2000) 706.
[59] Y. Watanabe, S. Kinoshita, J. Lumin. 87 (9) (2000) 895.
[60] S. Kinoshita, Y. Kai, Y. Watanabe, Chem. Phys. Lett. 301 (1999) 183.
[61] J. Wiedersich et al., J. Phys.: Condens. Matter 11 (1999) A147.
[62] J. Wiedersich, N.V. Surovtsev, E. Rossler, J. Chem. Phys. 113 (2000) 1143.
[63] W. P. de Boeij, thesis Rijksuniversiteit Groningen, 1997. Available from: <http://irs.ub.rug.nl/ppn/16369012X>.
[64] A. Baltuska, thesis Rijksuniversiteit Groningen, 2000. Available from: <http://irs.ub.rug.nl/ppn/191261726>.
[65] J.K. Ranka et al., Opt. Lett. 22 (1997) 1344.
[66] E.T.J. Nibbering, K. Duppen, D.A. Wiersma, Phys. Rev. Lett. 66 (1991) 2464.
[67] W.P. de Boeij, M.S. Pshenichnikov, D.A. Wiersma, J. Chem. Phys. 233 (1998) 287.
[68] W.P. de Boeij, M.S. Pshenichnikov, D.A. Wiersma, J. Phys. Chem. 100 (1996) 11806.
[69] M.H. Cho, J.Y. Yu, Y. Nagasawa, S.A. Passino, G.R. Fleming, J. Phys. Chem. 100 (1996) 11944.
[70] G. Rosen, J. Avissar, Y. Geven, J. Baram, J. Phys. E: Sci. Instrum. 20 (1987) 571.
[71] C.A. Angell, Science 267 (1995) 1924.
[72] C.A. Angell, J.M. Sare, E.J. Sare, J. Phys. Chem. 82 (1978) 2622.
[73] P. Neu et al., J. Lumin. 76–77 (1998) 619.
[74] K. Lazonder, K. Duppen, D.A. Wiersma, J. Phys. Chem. B 104 (2000) 6468.
[75] W.P. de Boeij, M.S. Pshenichnikov, D.A. Wiersma, J. Chem. Phys. 105 (1996).
[76] L. Allen, J.H. Eberly, Optical Resonances and Two-Level Atoms, Wiley, New York, 1975.
[77] K. Lazonder, M.S. Pshenichnikov, D.A. Wiersma, The echo-peak shift does not resolve all the details of bath dynamics, in preparation.
[78] C. Minhaeng et al., J. Chem. Phys. 99 (1993) 2410.
[79] Y. Gu, A. Widom, P.M. Champion, J. Chem. Phys. 100 (1994) 2547.
[80] R. Kubo, M. Toda, N. Hashitsume, Statistical Physics, Springer, Berlin, 1985.
[81] D.W. Oxtoby, Annu. Rev. Phys. Chem. 32 (1981) 77.
[82] V.B. Nemtsov, I.I. Fedchenia, A.V. Kondratenko, J. Schroeder, Phys. Rev. E 60 (1999) 3814.
[83] D.R. Greig, G.C. Joy III, D.F. Shriver, J. Chem. Phys. 67 (1977) 3189.
[84] A. Tokmakoff, B. Sauter, M.D. Fayer, J. Chem. Phys. 100 (1994) 9035.
[85] D.J. Myers, M. Shigeiwa, B.J. Cherayil, M.D. Fayer, J. Chem. Phys. 115 (2001) 4689.
[86] T.J. Kang, J.W. Yu, M. Berg, Chem. Phys. Lett. 174 (1990) 476.
[87] J.W. Yu, T.J. Kang, M. Berg, J. Chem. Phys. 94 (1991) 5787.
[88] J. Ma, D.V. Bout, M. Berg, J. Chem. Phys. 103 (1995) 9146.
[89] J. Ma, J.T. Fourkas, D.A. VandenBout, M. Berg, Supercooled Liq. 676 (1997) 199.
[90] M.A. Berg, Y.H. Zhang, M. Somoza, M.I. Sluch, Abstr. Am. Chem. Soc. 220 (2000) U195.
[91] Y.H. Zhang, M.A. Berg, J. Chem. Phys. 115 (2001) 4223.
[92] Y.H. Zhang, M.A. Berg, J. Chem. Phys. 115 (2001) 4231.
[93] Y.H. Zhang, M.I. Sluch, M.M. Somoza, M.A. Berg, J. Chem. Phys. 115 (2001) 4212.
[94] Y.H. Zhang, J.W. Jiang, M.A. Berg, J. Chem. Phys. 118 (2003) 7534.
[95] J.R. Schmidt, S.A. Corcelli, J.L. Skinner, J. Chem. Phys. 123 (2005) 044513.
[96] T.J. Aartsma, D.A. Wiersma, Phys. Rev. Lett. 36 (1976) 1360.